Design of Time Domain Equalizers Incorporating Radio Frequency Interference Suppression

Ya-Wen Wu

Advisor: Dr. Yuan-Pei Lin
Department of Electrical and Control Engineering
National Chiao Tung University

August 17, 2006

Abstract

It is known that radio frequency interference (RFI) degrades the performance of DMT systems for digital subscriber loops. The RFI signal, though narrow band in nature, may be spread to subchannels around the RFI frequencies due to the large sidelobes of the receiving rectangular window. In this thesis, we propose a joint consideration of channel shortening and RFI suppression in the design of time domain equalizers (TEQ). We will design the TEQ by minimizing ISI, channel noise and RFI interference. Simulation results are given to show that the proposed method can considerably reduce interference around the RFI frequencies and increase the transmission rate.

Contents

List of Figures

List of Tables

Chapter 1

Introduction

Discrete multitone (DMT) modulation is a very useful method for high-speed data transmission, e.g., asymmetric digital subscriber lines (ADSL) and very high speed digital subscriber lines (VDSL) [1][2]. The transmitter and receiver perform M-point inverse DFT (IDFT) and DFT computation, respectively, where M is the number of subchannels. For every block of M data samples, the transmitter adds a cyclic prefix (CP) of length ν. If the number ν is chosen to be no smaller than the order of the channel, then interblock interference (IBI) can be easily removed. The DFT outputs are multiplied with a set of scalars, known as the frequency domain equalizers (FEQ).

Usually the channel is longer than ν and the receiver includes a TEQ to shorten the channel impulse response. Many TEQ designs have been proposed [3]-[8]. In [3], Melsa *et al.* design the optimal TEQ that minimizes the out-of-window energy of the equivalent channel to minimizes IBI. In [4], Arslan *et al.* minimize ISI and channel noise on the tones used for transmission to design the TEQ. Per-tone equalization for bit rate maximization is proposed in [5]. A filterbank approach to the design of TEQ for maximizing the bit rate is given in [7]. A blind method to minimize the mean square error between the last sample and the corresponding sample of CP in adaptive way is given in [6]. A comprehensive overview on TEQ and a unified design approach is available in [8].

In the conventional DFT based multicarrier system the transmitting and receiving filters come from rectangular windows, which are known to have large spectral sidelobes. The stopband attenuation is insufficient for many applications. For example, poor frequency separation at the transmitter side leads to significant spectral leakage. This could pose a problem in applications where the PSD (power spectral density) of the transmit signal is required to have a large roll-off in certain frequency bands. In some wired transmission application, the PSD of the downstream transmit signal needs to fall below a threshold in the frequency bands of upstream transmission to avoid interference [1, 2]. The PSD should also be attenuated in amateur radio bands to reduce interference or egress emission [2]. On the other hand, poor frequency separation at the receiver side results in poor out-of-band rejection. In DMT application such as ADSL and VDSL, some of the frequency bands are also used by radio transmission systems, e.g., amplitude-modulation (AM) stations and amateur radio. These radio frequency signals can be coupled into the wires and interfere; they are known as RFI ingress [9]. The large sidelobe of the rectangular window in conventional multicarrier systems lead to spectral leakage. As a result, many neighboring tones can be affected. The signal to interference noise ratio of these tones are reduced and the total transmission rate is decreased. To improve RFI suppression, receiver windowing have been proposed in [9]-[11]. A combination of a raised-cosine window and per tone equalization are proposed to mitigate RFI interference in [12]. For the suppression of sidelobes without using extra redundant samples, it is proposed in [11] to use windows that introduced controlled IBI, later removed using decision feedback. Joint consideration of RFI and channel noise is considered in [10], the optimal window can be found using the statistics of the received RFI and noise. Joint design of TEQ and the receiving window for maximizing bit rate is given in [13]. In [13], it provides a general framework where a combined window and TEQ can be designed to maximize the bit rate for a given number of TEQ and window taps. The techniques of using dummy tones to reduce RFI is

proposed in [14]. The method to find the parameters that determine the shapes of the RFI signal are given in [15]. A channel independent window that minimizes output interference is given in [16], it provides a optimal receiver window design.

In this work, we propose a filterbank framework to the design of TEQ. we consider a joint optimization of channel shortening and RFI suppression. We will design the TEQ by minimizing ISI, channel noise and RFI interference. We will see that the proposed TEQ can significantly alleviate the effect of RFI for the tones around RFI frequencies. Simulation results are given to show that the proposed method can considerably reduce interference and achieve a higher transmission rate. Moreover, we will show the results of channel shortening.

Outline

The thesis is organized as follows. In chapter 2, we introduce the system model and the noise generations for VDSL system. In chapter 3, we give a briefly introduction of some exiting TEQ design methods and RFI suppression methods. The introductions including the method of Maximizing the shortening SNR [3], the method for bit rate optimal [7], the receiver window design based on filterbank structure [16] and joint consideration of TEQ and the receiving window design [13]. We present our proposed TEQ design method in chapter 4. Numerical simulations are shown in chapter 5 and a conclusion is given in chapter 6.

1.1 Notations

- Bold face upper case letters represent matrices. Bold face lower case letters represent vectors. $\mathbf{A}_T$ denotes transpose of $\mathbf{A}$, and $\mathbf{A}_{dagger}$ denotes conjugate transpose of $\mathbf{A}$.
- $\|\mathbf{x}\|$ denotes 2-norm of vector $\mathbf{x}$.
- The function $E[x]$ denotes the average value or expect value of x.

- $eig(\mathbf{A})$ is the operation of finding eigenvalues of $\mathbf{A}$.
- $*$ denotes the linear convolution operator, and $\star$ denotes the complex conjugate operator.
- M is the DFT size, ν is the CP length, $N = M+\nu$ is the transmitted symbol size, T is the TEQ length, L is the channel length, d is the synchronization delay, and T_s is the sampling rate.
- The notation $\mathbf{I}_m$ represents an $m \times m$ matrix.

Chapter 2

System Model

Very-high speed digital subscriber line (VDSL) transmits data by means of discrete multitone (DMT) system. In this chapter, the DMT system along with the system model will be introduced. In addition, we will present the filterbank representation of the DMT system.

2.1 DMT system

The DMT system is a popular method for high-speed data transmission for wired DSL (digital subscriber loops) applications. With a proper insertion of guard interval called cyclic prefix, an FIR channel can be decomposed into M parallel AGN subchannels with a gain that depends on the channel. In DMT transceiver, the transmitter and receiver perform respectively M-point inverse DFT (IDFT) and DFT computation, where M is the number of tones or number of subchannels. The P/S (parallel to series) converts parallel samples into series. For every block of M data samples, the transmitter adds a cyclic prefix (CP) of length ν in front of block, and CP is the last ν samples of the transmitted block. In practical implementation, DFT and IDFT are implemented digitally. Therefore, D/C and C/D converters are needed to work before the $M + \nu$ samples pass through physical channel and CP removal operation. In contrast to transmitter side, CP removal, S/P (series to parallel) and M-pt DFT are performed consecutively in

receiver side. Besides, if CP length ν is chosen to be no smaller than the order of the channel, then interblock interference (IBI) can be easily removed. The DFT output are multiplied with a set of scalars, known as the frequency domain equalizers (FEQs). The block diagram of DMT system is shown in Fig. 2.1.

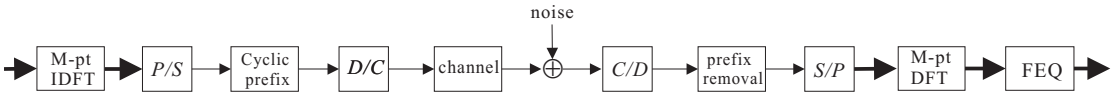

Figure 2.1: Traditional DMT scheme.

In DMT scheme, the efficiency of the transceiver is reduced by a factor of $\frac{M}{M+\nu}$, the larger the channel order is, the longer the cyclic prefix is needed to eliminate ISI, and the lower the efficiency is. To alleviate this problem in DSL application, a time domain equalizer (TEQ) is inserted to shorten the effective channel impulse response. From the input of D/C at the transmitter to the output of C/D at the receiver, we can represent it as a equivalent discrete time channel model in Fig. 2.2. $h_{eff}(n) = T_s h_c(nT_s)$, where T_s is the sampling rate.

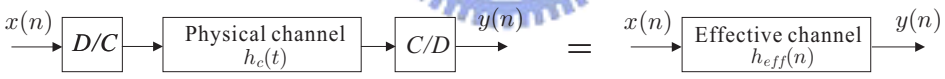

Figure 2.2: Effective discrete time channel.

Fig. 2.4 shows the equivalent discrete time DMT system model with TEQ added at the receiver, where $v(n)$ is the additive white Gaussian noise (AWGN) and $u(n)$ is the radio interference, they will be described in detail in section 2.3. The shortened channel becomes $c(n) * t(n)$. Let $\lambda(n)$ be the part of $c(n) * t(n)$ within a window of $\nu + 1$ samples where the energy is most concentrated. We can write

$$\lambda(n) = g(n)(c(n) * t(n)).$$

The window function $g(n)$ is given by

$$g(n) = \begin{cases} 1, & d \le n \le d + \nu, \\ 0, & \text{otherwise}, \end{cases} \tag{2.1}$$

where d is the synchronization delay. The sketch map is shown in Fig. 2.3.

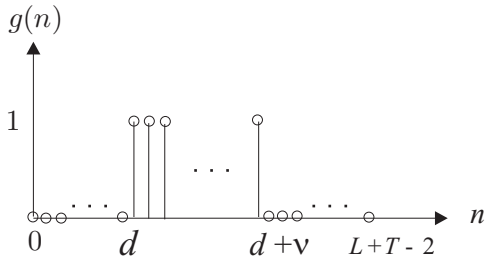

Figure 2.3: The coefficients of $g(n)$.

The scalar multiplier $1/P_k$ are known as the frequency domain equalizers, where

$$P_k = \Lambda(z)\,|_{z=e^{j2\pi k/M}},$$

where $\Lambda(z)$ is the z-transform of $\lambda(n)$.

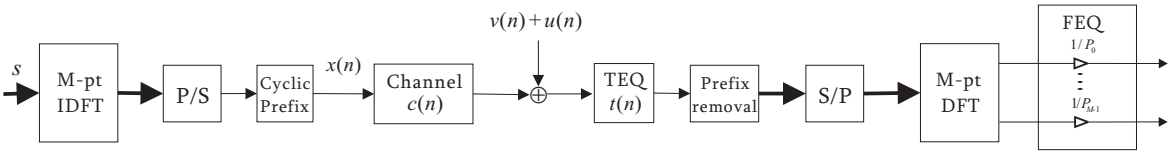

Figure 2.4: Equivalent discrete time DMT system model with TEQ.

2.2 Filterbank Representation

To facilitate the analysis, we use a filterbank (FB) representation and redraw the receiver structure as shown in Fig. 2.6. Before getting the sub-band filters $H_i(z)$, for $i = 0, 1, \ldots, M-1$, we translate the receiver structure in Fig. 2.4 into Fig. 2.5

first. The matrices $\mathbf{B}$ and $\mathbf{W}$ are the matrix representations of prefix removal and M-pt DFT operation. The dimensions of $\mathbf{B}$ and $\mathbf{W}$ are $M \times N$ and $M \times M$, respectively.

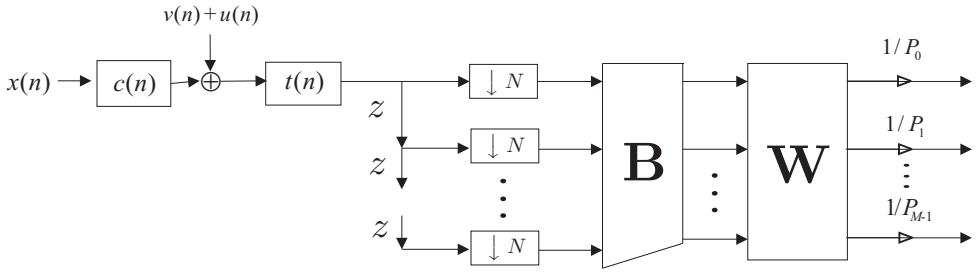

Figure 2.5: Matrix representation of the DMT receiver.

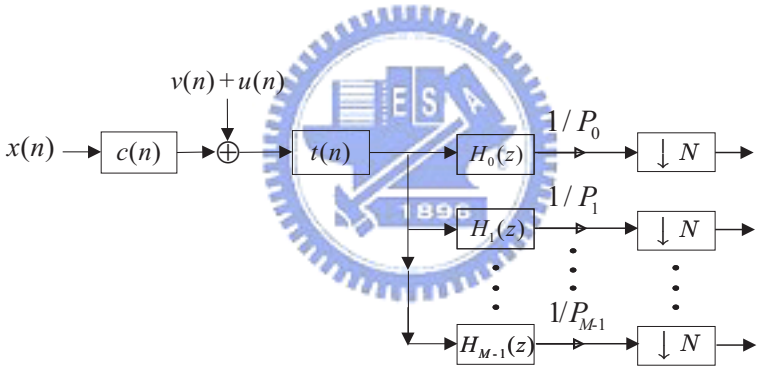

Figure 2.6: Filterbank representation of DMT receiver.

$$\mathbf{B} = (\ \mathbf{0} \quad \mathbf{I}_M\ ),$$

$$\mathbf{W} = \frac{1}{\sqrt{M}} \begin{pmatrix} 1 & 1 & \dots & 1 \\ 1 & W & \dots & W^{M-1} \\ \vdots & \vdots & \ddots & \vdots \\ 1 & W^{M-1} & \dots & W^{(M-1)^2} \end{pmatrix},$$

where $W = e^{-j\frac{2\pi}{M}}$.

Using multirate identities [17], the operations of prefix removal, serial to parallel (S/P) conversion and the M-pt DFT matrix in Fig. 2.4 can be redrawn as Fig. 2.6, where $N = M + \nu$. Due to the entries of matrices $\mathbf{B}$ and $\mathbf{W}$ are constant, it doesn't affect the results to change the order of decimator and these two operations. Connecting the equality relation between Fig. 2.5 and Fig. 2.6, we could obtain the $H_i(z)$ for $i = 0, 1, \ldots, M-1$ by the following derivation.

$$\begin{pmatrix} H_0(z) \\ H_1(z) \\ \vdots \\ H_{M-1}(z) \end{pmatrix} = \mathbf{WB} \begin{pmatrix} 1 \\ z \\ \vdots \\ z^{N-1} \end{pmatrix}. \tag{2.2}$$

From the above equation, it is not difficult to obtain the M receiving filters $H_i(z) = W^{-i\nu} H_0(zW^i)$, for $i = 0, 1, \ldots, M-1$, where $H_0(z) = \sum_{k=\nu}^{N-1} z^k$, and $W = e^{-j\frac{2\pi}{M}}$.

If multiple TEQs are used, one for each subchannel, the receiver becomes the one shown in Fig. 2.7 [7]. Now the effective channel for the k-th subchannel is $c(n) * t_k(n)$. Let $\lambda_k(n)$ be the part of $c(n) * t_k(n)$ inside the window, i.e.,

$$\lambda_k(n) = g(n)(c(n) * t_k(n)).$$

The k-th FEQ coefficient P_k is given by

$$P_k = \Lambda_k(z) \mid_{z=e^{j2\pi k/M}},$$

where $\Lambda_k(z)$ is the z-transform of $\lambda_k(n)$.

We note that if the order of the shortened channel $C(z)T_k(z)$ is not larger than cyclic prefix length, the DMT system still has ISI free property. Also, by setting $T_k(z) = T(z)$ for $k = 0,\ 1,\ \ldots,\ M-1$, then Fig. 2.7 reduces to the case in Fig. 2.6.

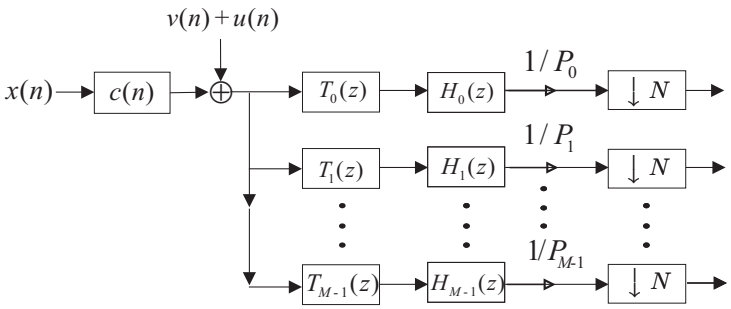

Figure 2.7: DMT receiver with multiple TEQs.

2.3 Generation of Noise for the VDSL system

The VDSL environment on the copper twisted-pair lines is influenced by several additive noise impairments, including a white noise, a crosstalk coupled from adjacent loops in the cable bundle between receiver and transmitter and radio frequency interference (RFI). The additive Gaussian white noise is the electronic noise caused by the material property of the twist-pair cable. By definition, crosstalk is due to adjacent lines in a bundle that are improperly shielded from each other, and therefore the signals from other lines are electro-magnetically coupled to the considered line and cause interference. Crosstalk can be separated into two categories: NEXT (Near-End Crosstalk) and FEXT (Fear-End Crosstalk). NEXT occurs when a receiver detects other signals in the same bundle from transmitters that are located in proximity, while FEXT occurs when the other detected signals are from remote transmitters, located at the other end of the bundle. Another part of the noise in the VDSL environment is the radio frequency interference (RFI). The RFI mainly comes from radio amateurs and broadcast AM radio, which overlap VDSL bands. In this section, we will generate three different kinds of noise, additive white Gaussian noise (AWGN), Far-End crosstalk (FEXT) and the other is radio interference in VDSL system [2]. The Near-End crosstalk (NEXT) can be generated following the same step as FEXT

noise.

2.3.1 AWGN (Additive White Gaussian Noise)

Take DFT size is M, and CP length is ν for example. The sampling frequency is F_s MHz, and the sampling period is $T_s = 1/F_s$. Suppose the continuous AWGN PSD is N_0 dBm/Hz and it is measured across a terminal resistor R_v Ohm. The continuous white noise PSD can be rewritten in measurement of voltage.

$$S_c(j\Omega) = 10^{N_0/10} \cdot 10^{-3} \cdot R_v \quad (V^2). \tag{2.3}$$

Assume the magnitude response of antialiasing filter before the C/D converter $|H_a(j\Omega)| = 1 \ \ \forall\, |\Omega| < \frac{\pi}{T_s}$. The discrete white noise PSD is

$$S_d(e^{j\omega}) = S_c(j\Omega) \cdot F_s \cdot |H_a(j\Omega)| \quad (dB) \tag{2.4}$$

The PSD of continuous white noise and discrete white noise in our analysis are shown in Fig. 2.8. The relevant parameters are setting as follows: $M = 1024$, $\nu = 80$, $F_s = 4.416$MHz, $N_0 = -140$dBm/Hz and $R_v = 100$Ohm.

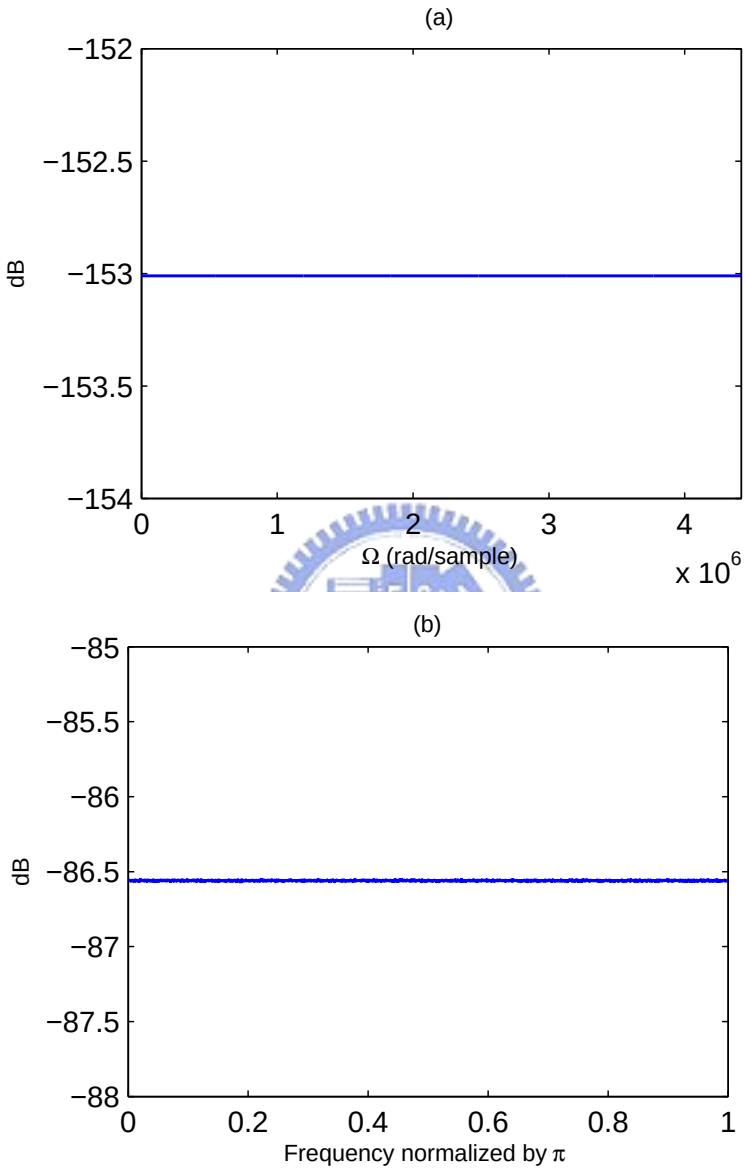

Figure 2.8: (a) Continuous time white noise PSD $S_c(j\Omega)$. (b) Discrete time white noise PSD $S_d(e^{j\omega})$.

2.3.2 Crosstalk Noise

The most important noise mechanism in pair cables is interference from other pairs in the cable, which is denoted crosstalk. There are two types of crosstalk, near-end crosstalk (NEXT), which is interference between opposite direction of transmission, and far-end crosstalk (FEXT), which is defined as a measure of the unwanted signal coupling from a transmitter at the near-end into a neighboring pair measured at the far-end. There is a sketch map in Fig. 2.9.

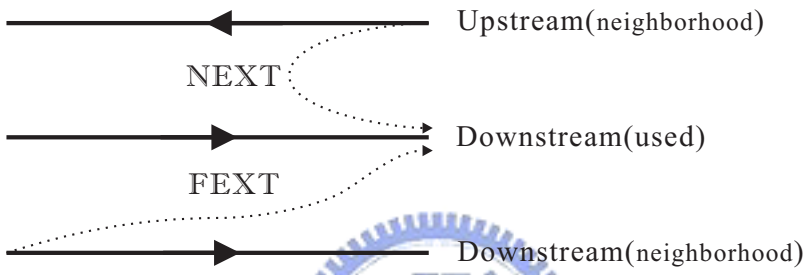

Figure 2.9: The sketch map of FEXT and NEXT noise.

The specification of FEXT noise in VDSL system is described in detail in VDSL standard [2]. The FEXT noise generator is shown in Fig. 2.10. The PSD

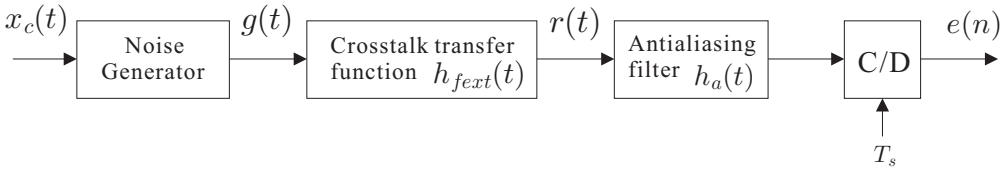

Figure 2.10: FEXT noise generator.

of $g(t)$ is equal to the PSD of $x(t)$, $S_{x_c}(j\Omega)$, plus 8 dB, where $S_{x_c}(j\Omega)$ is the transmission power spectral density.

$$S_g(j\Omega) = S_{x_c}(j\Omega) \cdot 10^{0.8} \quad (V^2), \tag{2.5}$$

and it is measured across a terminal resistor R_v Ohm. The addition of 8 dB approximates the power generated by the sum of 20 VDSL system operating

in a multi-pair cable. The magnitude response of crosstalk transfer function $H_{fext}(j\Omega, L)$ is

$$|H_{fext}(j\Omega, L)|^2 = |H(j\Omega, L)|^2 \cdot K_{fext} \cdot (1/49)^{0.6} \cdot L \cdot (\Omega/2\pi)^2, \tag{2.6}$$

where $|H(j\Omega, L)|$ is the magnitude of channel frequency response, the crosstalk coupling coefficient $K_{fext} = 2.44 \times 10^{-22}$ for category-5 twisted pair and L (feet) is the length of twisted pair loop. The PSD of discrete FEXT noise $e(n)$ is

$$S_e(e^{j\omega}) = \frac{1}{T_s} \cdot S_r(j\frac{\omega}{T_s}), \quad |\,\omega| \leq \pi \tag{2.7}$$

However, we can generate discrete FEXT noise by implementing a random process shown as Fig. 2.11. That is,

$$S_e(e^{j\omega}) = S_z(e^{j\omega}) \cdot \left|H_f(e^{j\omega})\right|^2 \tag{2.8}$$

where $S_z(e^{j\omega})$ is the PSD of $z(n)$. Our goal is to generate a random sequence with PSD $S_e(e^{j\omega})$ as in (2.7). If $S_z(e^{j\omega}) = 1$, then $|H_f(e^{j\omega})|^2 = S_e(e^{j\omega})$. Thus, the FIR filter $h_f(n)$ can be obtained from IDFT of the square root of $S_e(e^{j\omega})$ over $\omega = \{0 \sim 2\pi\}$. In next examples, we use VDSL loop 1 long of 4500 ft as the

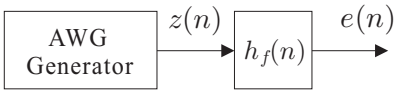

Figure 2.11: Simplified FEXT noise generator.

channel. The DFT size $M = 1024$ and CP length $\nu = 80$.

Fig. 2.12(a) shows the magnitude response of channel $|H(j\Omega, L)|^2$ in (2.6) and Fig. 2.12(b) shows the crosstalk transfer function $|H_{fext}(j\Omega, L)|^2$ in (2.6). Fig. 2.12(c) shows the PSD of continuous time FEXT noise $S_r(j\frac{\omega}{T_s})$ in (2.7) and Fig. 2.12(d) shows the PSD of discrete time FEXT noise $S_e(e^{j\omega})$ in (2.7). Fig. 2.12(e) shows the PSD of the equivalent FEXT noise $S_e(e^{j\omega})$ in (2.8) obtained by processing Fig. 2.11.

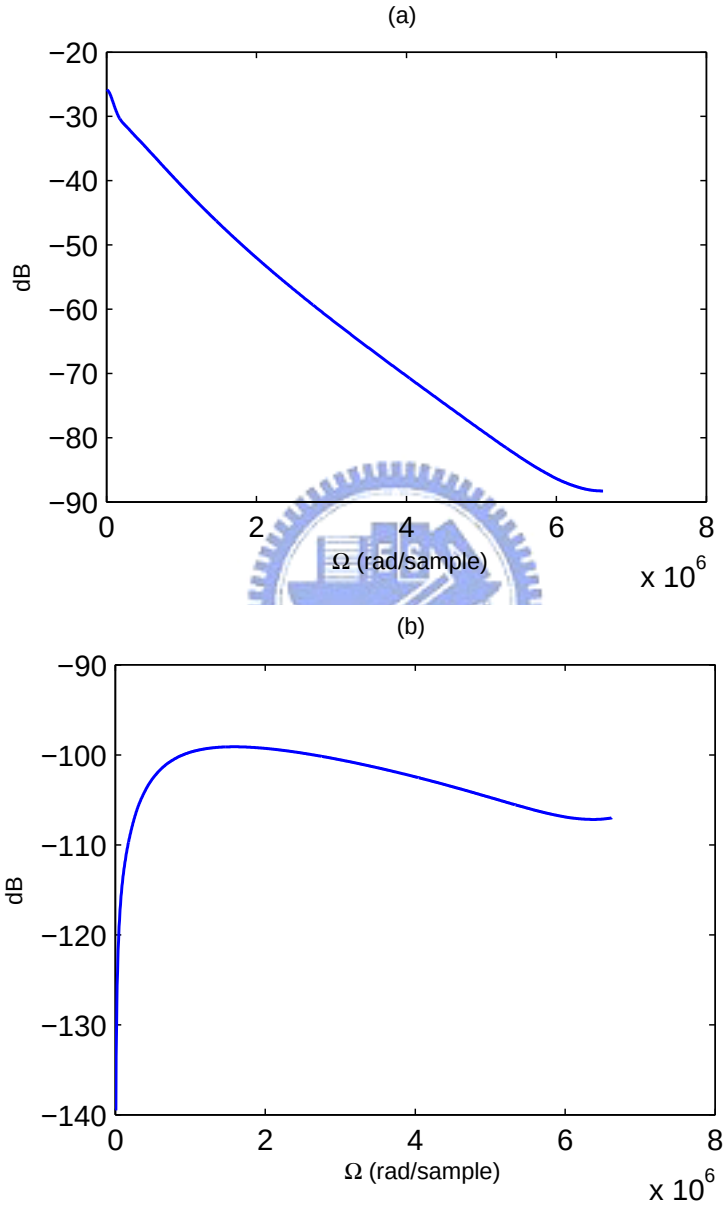
(a)
−20
−30
−40
−50
−60
−70
−80
−90
dB
0
2
4
6
8
Ω (rad/sample)
x 10^6
(b)
−90
−100
−110
−120
−130
−140
dB
0
2
4
6
8
Ω (rad/sample)
x 10^6

(c)

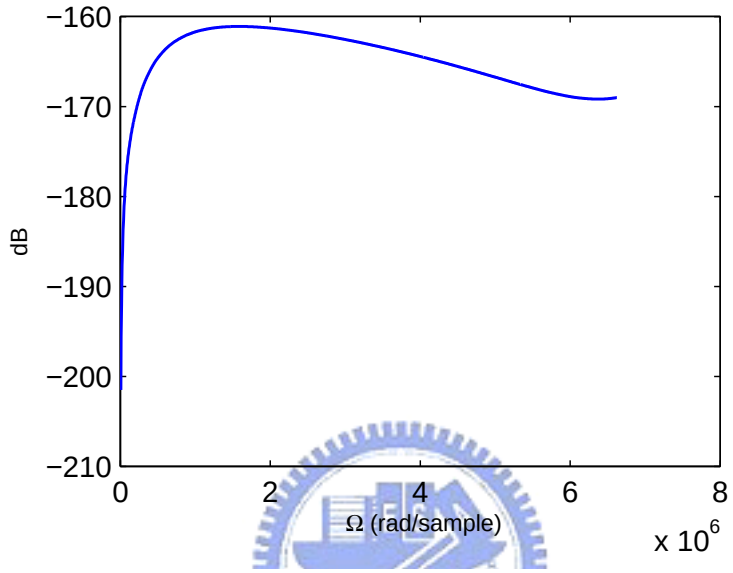
−160
−170
−180
−190
−200
−210
dB
0
2
4
6
8
Ω (rad/sample)
x 10^6

(d)

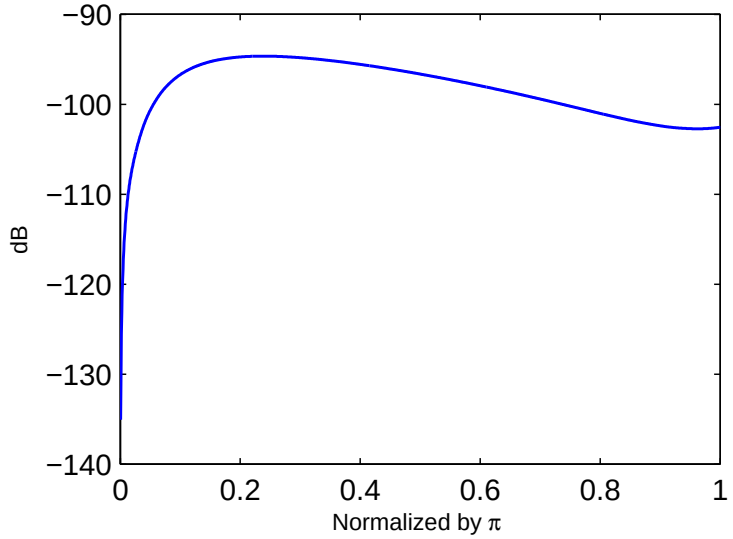
−90
−100
−110
−120
−130
−140
dB
0
0.2
0.4
0.6
0.8
1
Normalized by π

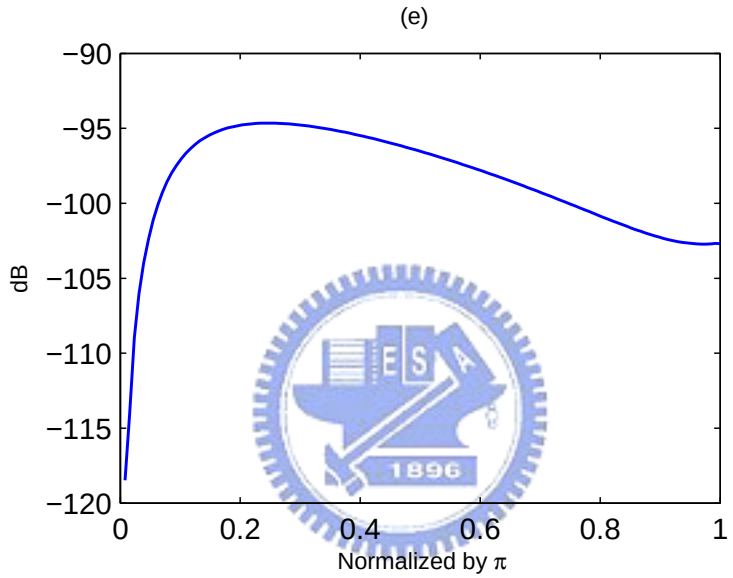

Figure 2.12: (a) The magnitude response of channel $|H(j\Omega, L)|^2$, (b) the magnitude response of crosstalk transfer function $|H_{fext}(j\Omega, L)|^2$, (c) the PSD of continuous time FEXT noise $S_r(j\Omega)$, (d) the PSD of discrete time FEXT noise $S_e(e^{j\omega})$, (e) the PSD of FEXT noise generated by passing a white Gaussian sequence through the filter $h_f(n)$.

2.3.3 RFI (Radio Frequency Interference)

The VDSL transmission system shares its spectrum with different types of radio transmission, ranging from medium- and short-wave amplitude- modulated (AM) stations, over public safety and distress bands, to amateur radio. As a result of the cable imbalance, these radio frequency (RF) signals can be received by telephone wires and interfere with the VDSL signal at the receiving side. This type of noise in a VDSL transmission system is known as RF interference (RFI) ingress [9].

When the RFI signal $u_c(t)$ is a amplitude-modulation (AM) signal [2], we have

$$u_c(t) = A_c \cdot [1 + a \cdot m(t)] \cdot cos(\Omega_c t + \theta(t)), \tag{2.9}$$

where a is a constant called the amplitude sensitivity of the modulator responsible for the generation of the modulation signal $u_c(t)$, A_c is the carrier amplitude, $m(t)$ is the message signal, and Ω_c and $\theta(t)$ are respectively the frequency and phase of interference source. In [2], it is assumed that the AM broadcast sources shall be modeled by a fixed frequency carrier 30% AM modulated with a flat ($\pm$ 3dB) Gaussian noise source band limited to 0-5 KHz, so that let $a = 3/10$ and $m(t)$ is a zero-mean random signal with PSD $S_m(f)$ is 3 dB over bandwidth 5 KHz, the variance of $m(t)$ can be determined from

$$\sigma_m^2 = \int_{-\infty}^{\infty} S_m(f)\ df = 10^3 \int_{-5/2}^{5/2} 2\ df = 10^4 \quad (V^2), \tag{2.10}$$

and $\theta(t)$ is a uniform distribution random signal, the cumulative distribution function (cdf) is

$$f_\theta(t) = \begin{cases} 1/2\pi & |t| \le \pi, \\ 0 & \text{otherwise.} \end{cases} \tag{2.11}$$

The coefficient A_c can derived by the following step. The autocorrelation function of $u_c(t)$ is

$$R_{u_c}(t_1 - t_2) = E[u_c(t_1)u_c^*(t_2)] = \frac{1}{2} \cdot A_c^2 \cdot cos(\Omega_c \tau) \cdot [1 + a^2 \cdot R_m(\tau)], \tag{2.12}$$

where $\tau = t_1 - t_2$. Therefore, we can obtain the PSD of $u_c(t)$ by performing Fourier Transform on (2.12), that is,

$$S_{u_c}(f) = \frac{1}{2}A_c^2 \cdot [\pi(\delta(f - f_c) + \delta(f + f_c)) + \frac{1}{2}a^2(S_m(f - f_c) + S_m(f + f_c))] \quad (2.13)$$

the variance of $u_c(t)$ is

$$\sigma_{u_c}^2 = \int_{-\infty}^{\infty} S_{u_c}(f)\, df = A_c^2 \cdot [\pi + \frac{1}{2}a^2 \cdot \sigma_m^2] \quad (V^2). \quad (2.14)$$

Let us take the differential mode with strength -55 dBm (the distance between client and interference source is 6000 ft) for example. Assume the across terminal resistor $R_v = 100$ Ohm, the receiving RFI power is measured by

$$10^{0.1\times(-55)} \times 10^{-3} = \frac{\sigma_{u_c}^2}{R_v} \quad (watt). \quad (2.15)$$

Applying (2.14) to (2.15), we can obtain (2.16), and find the carrier amplitude A_c as in (2.17).

$$A_c^2 \cdot [\pi + \frac{1}{2}a^2 \cdot \sigma_m^2] = R_v \cdot 10^{-3} \cdot 10^{0.1\times(-55)}. \quad (2.16)$$

$$A_c = \sqrt{\frac{R_v \cdot 10^{(-5.5-3)}}{\pi + \frac{1}{2}a^2 \cdot \sigma_m^2}} = 2.6417 \times 10^{-5}. \quad (2.17)$$

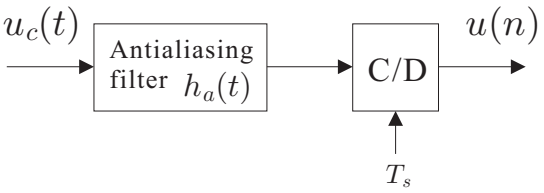

Figure 2.13: RFI noise generator.

The discrete time RFI signal is generated as Fig. 2.13. The discrete signal $u(n)$ is obtained by sampling the continuous time signal $u_c(t)$.

$$u(n) = A_c \cdot [\ 1 + a \cdot m(nT_s)] \cdot cos(\Omega_c \cdot nT_s + \theta(nT_s))$$

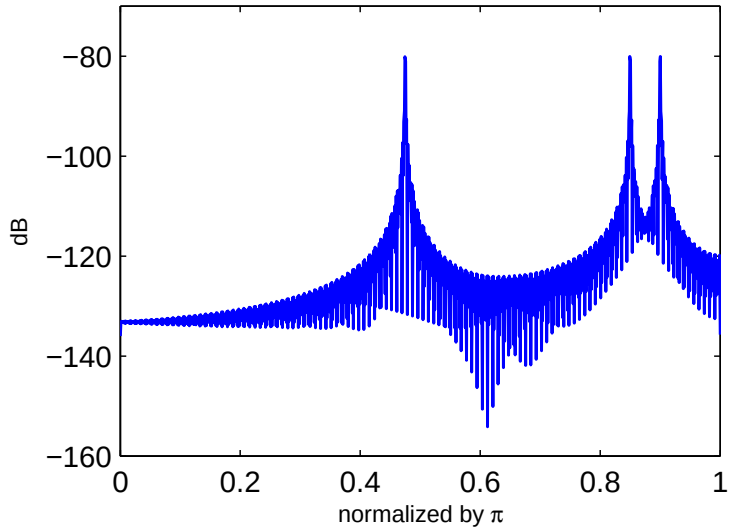

Figure 2.14: The magnitude response of discrete time RFI noise.

$$= A_c \cdot [\ 1 + a \cdot m(nT_s)] \cdot cos(\omega_c n + \theta(nT_s)). \tag{2.18}$$

Fig. 2.14 shows the magnitude response of discrete time RFI signal. The discrete time RFI signal is windowed by a rectangular window, and then M-pt DFT is performed. The Fourier transform of rectangular window is a sinc-like function, and it has large sidelobe. The test frequencies of RFI sources are at 1.05MHz, 1.9MHz and 2.0MHz. We can see Fig. 2.14 shows the effect of sidelobe due to windowing.

Chapter 3

Previous design methods

In this chapter, we will give a survey of some existing design methods for TEQ and RFI suppression. In particular, we will introduce the TEQ design methods of maximizing shortening SNR [3] and bit-rate optimized [7] in section 3.1. The methods of receiver window design based on filterbank structure [16] and joint window and TEQ design [13] for RFI suppression are also introduced in section 3.2.

3.1 Previous TEQ designs

3.1.1 Maximize the shortening SNR

The MSSNR technique is to maximize the ratio of the energy in the largest consecutive $\nu + 1$ samples of effective channel to the energy in the remaining samples, where ν is the CP length. In [3], it derived the SIR as a quadratic form and solve the optimal solution by solving eigen problem.

The equivalent channel $h_{eff}(n) = c(n) * t(n)$, and the coefficients of $h_{eff}(n)$ can be represented as $\mathbf{h}_{eff} = \mathbf{Ct}$, where $\mathbf{C}$ is a convolution matrix, composed of the original channel coefficients, and $\mathbf{t}$ is a $T \times 1$ vector, composed of TEQ

coefficients.

$$\mathbf{h}_{eff} = \begin{pmatrix} h_{eff}(0) \\ h_{eff}(1) \\ \vdots \\ h_{eff}(L+T-2) \end{pmatrix}$$

$$= \begin{pmatrix} c(0) & 0 & \dots & \dots & 0 \\ c(1) & c(0) & \dots & \dots & 0 \\ \vdots & \ddots & \ddots & \dots & \vdots \\ c(L-1) & c(L-2) & \dots & c(L-T+1) & c(L-T) \\ 0 & c(L-1) & \dots & \dots & c(L-T+1) \\ \vdots & \ddots & \dots & \dots & \vdots \\ 0 & 0 & \dots & 0 & c(L-1) \end{pmatrix} \begin{pmatrix} t(0) \\ t(1) \\ \vdots \\ t(T-1) \end{pmatrix} \quad (3.1)$$

Let $\mathbf{h}_{win}$ represent a window if $\nu+1$ consecutive samples of $\mathbf{h}_{eff}$ starting with sample d, and let $\mathbf{h}_{wall}$ represent the remaining $L+T-\nu-2$ samples of $\mathbf{h}_{eff}$.

$$\mathbf{h}_{win} = \begin{pmatrix} h_{eff}(d) \\ h_{eff}(d+1) \\ \vdots \\ h_{eff}(d+\nu) \end{pmatrix}$$

$$= \begin{pmatrix} c(d) & c(d-1) & \dots & c(d-T+1) \\ c(d+1) & c(d) & \dots & c(d-T+2) \\ \vdots & & \ddots & \vdots \\ c(d+\nu) & c(d+\nu-1) & \dots & c(d+\nu-T+1) \end{pmatrix} \begin{pmatrix} t(0) \\ t(1) \\ \vdots \\ t(T-1) \end{pmatrix} \equiv \mathbf{C}_{win}\mathbf{t} \quad (3.2)$$

$$\mathbf{h}_{wall} = \begin{pmatrix} h_{eff}(0) \\ \vdots \\ h_{eff}(d-1) \\ h_{eff}(d+\nu+1) \\ \vdots \\ h_{eff}(L+T-2) \end{pmatrix}$$

$$= \begin{pmatrix} c(0) & 0 & \dots & 0 \\ \vdots & \ddots & & \\ c(d-1) & c(d-2) & \dots & c(d-T) \\ c(d+\nu+1) & c(d+\nu) & \dots & c(d+\nu-T+2) \\ \vdots & \ddots & & \\ 0 & \dots & 0 & c(L-1) \end{pmatrix} \begin{pmatrix} t(0) \\ t(1) \\ \vdots \\ t(T-1) \end{pmatrix} \equiv \mathbf{C}_{wall}\mathbf{t} \tag{3.3}$$

The ratio of the energy in the largest consecutive $\nu+1$ samples of effective channel to the energy in the remaining samples can be expressed as

$$\frac{\mathbf{h}_{win}^{\dagger}\mathbf{h}_{win}}{\mathbf{h}_{wall}^{\dagger}\mathbf{h}_{wall}} = \frac{\mathbf{t}^{\dagger}\mathbf{C}_{win}^{\dagger}\mathbf{C}_{win}\mathbf{t}}{\mathbf{t}^{\dagger}\mathbf{C}_{wall}^{\dagger}\mathbf{C}_{wall}\mathbf{t}} = \frac{\mathbf{t}^{\dagger}\mathbf{A}\mathbf{t}}{\mathbf{t}^{\dagger}\mathbf{B}\mathbf{t}}, \tag{3.4}$$

where $\mathbf{A} = \mathbf{C}_{win}^{\dagger}\mathbf{C}_{win}$ and $\mathbf{B} = \mathbf{C}_{wall}^{\dagger}\mathbf{C}_{wall}$. The optimal TEQ should be chosen to minimize $\mathbf{h}_{wall}^{\dagger}\mathbf{h}_{wall}$ while satisfying the constraint $\mathbf{h}_{win}^{\dagger}\mathbf{h}_{win} = 1$. The matrix $\mathbf{B}$ is Hermitian and positive semi-definite, but it is a rare case when the determinant of matrix $\mathbf{B}$ is zero. However, we can assume it is a positive definite matrix, thus it is invertible. The optimal TEQ can be obtained by maximizing (3.4), this is a eigen problem. The optimal TEQ $\mathbf{t}$ is the eigenvector of $\mathbf{B}^{-1}\mathbf{A}$ corresponding to the maximum eigenvalue.

3.1.2 Bit-Rate Optimized TEQ Design

In this section, we review the TEQ design method for minimizing ISI and channel noise [4, 7]. Define $f_k(n) = (1 - g(n))(c(n) * t_k(n))$. The sketch map of $f_k(n)$ is shown in Fig. 3.1. The purpose of the definition of $f_k(n)$ is to find the output error caused by ISI and noise easily.

From Fig. 2.7, we see that the output error caused by ISI and noise at the kth tone is $e_k(n) = [e_{isi,k}(n) + e_{noise,k}(n)]_{\downarrow N}$, where

$$e_{isi,k}(n) = x(n) * f_k(n) * h_k(n)/P_k, \tag{3.5}$$

$$e_{noise,k}(n) = v(n) * t_k(n) * h_k(n)/P_k. \tag{3.6}$$

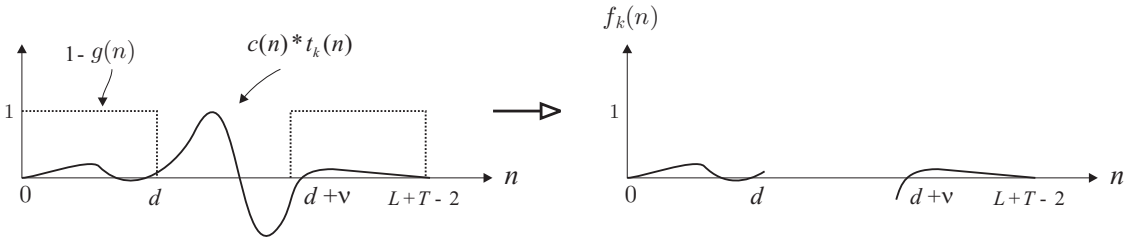

Figure 3.1: Illustration of $f_k(n)$.

Owing to the fact that the decimator does not change the signal variance, we have $\sigma_k^2 = \sigma_{isi,k}^2 + \sigma_{noise,k}^2$, where $\sigma_{isi,k}^2$ and $\sigma_{noise,k}^2$ are respectively the variances of $e_{isi,k}(n)$ and $e_{noise,k}(n)$. In this thesis, the signal and noise are assumed to be uncorrelated, and $x(n)$ is assumed to be a white WSS process for simplicity.

Let $\mathbf{t}_k$ be the $T \times 1$ column vector consisting of the k-th TEQ coefficients.

$$\mathbf{t}_k = (t_k(0)\ t_k(1)\ \ldots\ t_k(T-1))_{1\times T}^T.$$

The coefficients of $\lambda_k(n)$ can be written in a matrix form as $\mathbf{GCt}_k$, where $\mathbf{C}$ is an $(L+T-1)\times T$ lower triangular Toeplitz matrix, and $\mathbf{G}$ is a $(L+T-1)\times(L+T-1)$ diagonal with $[\mathbf{G}]_{ii} = g(i), i = 0,\ 1, \ldots,\ L+T-2$.

$$\mathbf{C} = \begin{pmatrix} c(0) & 0 & 0 & 0 & \ldots & 0 \\ c(1) & c(0) & 0 & 0 & \ldots & 0 \\ \vdots & \ddots & \ddots & \ddots & \ldots & \vdots \\ c(L-1) & \ldots & c(1) & c(0) & \ldots & 0 \\ \vdots & \ddots & \ddots & \ddots & \ddots & \vdots \\ 0 & 0 & \ldots & \ldots & c(L-1) & c(L-2) \\ 0 & 0 & \ldots & \ldots & 0 & c(L-1) \end{pmatrix}_{(L+T-1)\times T}, \tag{3.7}$$

$$\mathbf{G} = \begin{pmatrix} g(0) & & & \\ & g(1) & & 0 \\ & & \ddots & \\ & 0 & & g(L+T-2) \end{pmatrix}, \tag{3.8}$$

Let $\mathbf{w}_k$ be the first ν elements of the k-th row vector of the M-point DFT

matrix,

$$\mathbf{w}_k = (1 \; e^{-j\frac{2\pi}{M}k} \; \ldots \; e^{-j\frac{2\pi}{M}k(\nu-1)})_{1\times\nu}.$$

Then P_k can be written as $P_k = \mathbf{w}_k\mathbf{G}\mathbf{C}\mathbf{t}_k$ and thus $|P_k|^2 = \mathbf{t}_k^\dagger\mathbf{B}_k\mathbf{t}_k$, where

$$\mathbf{B}_k = \mathbf{C}^\dagger\mathbf{G}^\dagger\mathbf{w}_k^\dagger\mathbf{w}_k\mathbf{G}\mathbf{C}. \tag{3.9}$$

The coefficients of $f_k(n)$ can be written in a matrix form as $\mathbf{D}\mathbf{C}\mathbf{t}_k$, where $\mathbf{D}$ is diagonal, $\mathbf{D} = \mathbf{I} - \mathbf{G}$. Using matrix representation for convolution, we can write the coefficients of $f_k(n) * h_k(n)$ as $\mathbf{H}_k\mathbf{D}\mathbf{C}\mathbf{t}_k$, where $\mathbf{H}_k$ is an $(M+L+T-2)\times(L+T-1)$ lower triangular Toeplitz matrix with the first column given by

$$\left(e^{-j\frac{2\pi}{M}k(M-1)} \; e^{-j\frac{2\pi}{M}k(M-2)} \; \ldots \; 1 \; 0 \; \ldots \; 0\right)^T, \tag{3.10}$$

$$\mathbf{H}_k = \begin{pmatrix} e^{-j\frac{2\pi}{M}k(M-1)} & 0 & 0 & 0 & \ldots & 0 \\ e^{-j\frac{2\pi}{M}k(M-2)} & e^{-j\frac{2\pi}{M}k(M-1)} & 0 & 0 & \ldots & 0 \\ \vdots & \ddots & \ddots & \ddots & \ldots & \vdots \\ 1 & \ldots & e^{-j\frac{2\pi}{M}k(M-2)} & e^{-j\frac{2\pi}{M}k(M-1)} & \ldots & 0 \\ \vdots & \ddots & \ddots & \ddots & \ddots & \vdots \\ 0 & 0 & \ldots & \ldots & 1 & e^{-j\frac{2\pi}{M}k} \\ 0 & 0 & \ldots & \ldots & 0 & 1 \end{pmatrix}. \tag{3.11}$$

Using the matrix representation, the error variances caused by ISI can be rewritten as:

$$\sigma_{isi,k}^2 = \frac{\mathbf{t}_k^\dagger\mathbf{Q}_{isi,k}\mathbf{t}_k}{\mathbf{t}_k^\dagger\mathbf{B}_k\mathbf{t}_k}, \tag{3.12}$$

where $\mathbf{Q}_{isi,k} = \sigma_x^2\mathbf{C}^\dagger\mathbf{D}^\dagger\mathbf{H}_k^\dagger\mathbf{H}_k\mathbf{D}\mathbf{C}$. Similarly, we have $\sigma_{noise,k}^2$ in the following matrix form

$$\sigma_{noise,k}^2 = \frac{\mathbf{t}_k^\dagger\mathbf{Q}_{noise,k}\mathbf{t}_k}{\mathbf{t}_k^\dagger\mathbf{B}_k\mathbf{t}_k}, \tag{3.13}$$

where $\mathbf{Q}_{noise,k} = \tilde{\mathbf{H}}_k^\dagger\mathbf{R}_v\tilde{\mathbf{H}}_k$. The matrix $\mathbf{R}_v$ is the $(M+T-1)\times(M+T-1)$ autocorrelation matrix of $v(n)$ and $\tilde{\mathbf{H}}_k$ is an $(M+T-1)\times T$ lower triangular Toeplitz matrix whose first column is the same as in (3.10) except that the last $L-1$ zeros are discarded.

3.2 Previous design method for RFI suppression

3.2.1 Optimal Receiver Window Design

In this section, we will briefly review the method given in [16]. Assume μ is the window length. To apply windows, the receiver takes the $M+\mu$ samples, multiplies the first μ samples by window coefficients $w(n), n = 0,\ 1,\ \ldots,\ \mu-1$ and multiplies the last μ samples by $1-w(n)$. Assume $\mathbf{w} = [w_0 \cdots w_{\mu-1}]^T$ is the $\mu \times 1$ window coefficient vector. Now the matrix $\mathbf{B}$ in Fig. 2.5 is given by

$$\mathbf{B} = \begin{pmatrix} 0 & 0 & I_{M-L} & 0 \\ 0_{L\times(P-L)} & \mathbf{C} & 0 & \mathbf{D} \end{pmatrix}, \tag{3.14}$$

where

$$\mathbf{C} = \begin{pmatrix} w_0 & 0 & \cdots & 0 \\ 0 & w_1 & \ddots & \vdots \\ \vdots & \ddots & \ddots & 0 \\ 0 & \cdots & & w_{L-1}, \end{pmatrix} \tag{3.15}$$

$$\mathbf{D} = \mathbf{I}_L - \mathbf{C}. \tag{3.16}$$

The relation of the M receiving filter $H_k(z)$ for $k = 0,\ 1,\ \ldots,\ M-1$, $\mathbf{B}$ and $\mathbf{W}$ is given in (2.2), using the expression of $\mathbf{B}$ in (3.14), we can verify that the coefficients of the first receiving filter $h_0(n)$ are given by

$$h_0(n) = \begin{cases} w_{-n-\nu+\mu}, & -(\nu-1) \le n \le -(\nu-\mu) \\ 1, & -(N-\mu-1) \le n \le -\nu \\ 1 - w_{-n-N+\mu}, & -(N-1) \le n \le -(N-\mu) \\ 0, & \text{otherwise.} \end{cases} \tag{3.17}$$

The k-th receiving filter $H_k(z)$ is essentially a shifted version of $H_0(z)$.

We assume that RFI interference occurs at frequency ω_l with amplitude α_l and phase $\theta_l,\ l = 0, \cdots, R-1$. Thus we can model the interference as

$$u(n) = \sum_{l=0}^{R-1} \alpha_l \cos(\omega_l n + \theta_l). \tag{3.18}$$

The output of the i-th receiving filter comes from RFI interference is

$$\frac{1}{2}\sum_{l=0}^{R-1}\alpha_l[c_{l,i}e^{j(\omega_l n+\theta_l)}+c_{l,i}^{'}e^{-j(\omega_l n+\theta_l)}], \tag{3.19}$$

where $c_{l,i}=H_i(e^{j\omega_l})$ and $c_{l,i}^{'}=H_i(e^{-j\omega_l})$. To suppress the total interference, we can minimize

$$J=\sum_{l=0}^{R-1}\sum_{i=0,i\in U}^{M-1}\alpha_l^2[|c_{l,i}|^2+|c_{l,i}^{'}|^2] \tag{3.20}$$

where U is the set of tones that are used for transmission.

$$\begin{array}{l} c_{l,i}=W^{-i\nu}H_0(e^{j(\omega_l-2\pi i/M)}) \\ c_{l,i}^{'}=W^{-i\nu}H_0(e^{-j(\omega_l-2\pi i/M)}) \end{array} \tag{3.21}$$

From (3.17) we can verify that $H_0(e^{j(\omega_l-2\pi i/M)})$ can be given in terms of the window coefficients as

$$H_0(e^{j(\omega_l-2\pi i/M)})=b_{l,i}+\mathbf{a}_{l,i}^{\dagger}\mathbf{w}, \tag{3.22}$$

where $b_{l,i}$ is a scalar and $\mathbf{a}_{l,i}$ is a $\mu\times 1$ column vectors given respectively by

$$\begin{array}{rl} b_{l,i}= & \sum_{l=\nu}^{\nu+M-1}e^{j(\omega_l-2\pi i/M)l}, \\ [\mathbf{a}_{l,i}]_m= & e^{j(\omega_l-2\pi i/M)(\nu-\mu+m)} \\ & -e^{j(\omega_l-2\pi i/M)(N-\mu+m)}. \end{array} \tag{3.23}$$

Similarly, we can verify that $H_0(e^{-j(\omega_l+2\pi i/M)})$ can be expressed by

$$H_0(e^{-j(\omega_l+2\pi i/M)})=b'_{l,i}+\mathbf{a'}_{l,i}^{\dagger}\mathbf{w}, \tag{3.24}$$

where $b'_{l,i}$ and $\mathbf{a'}_{l,i}$ are respectively

$$\begin{array}{rl} b'_{l,i}= & \sum_{l=P}^{\nu+M-1}e^{-j(\omega_l+2\pi i/M)l}, \\ [\mathbf{a'}_{l,i}]_m= & e^{-j(\omega_l+2\pi i/M)(\nu-\mu+m)} \\ & -e^{-j(\omega_l+2\pi i/M)(N-\mu+m)}. \end{array} \tag{3.25}$$

Using (3.20) to (3.23), we can derive,

$$\begin{array}{rl} J= & \mathbf{w}^T(\mathbf{A}^{\dagger}\mathbf{A}+\mathbf{A'}^{\dagger}\mathbf{A'})\mathbf{w}+\mathbf{w}^T(\mathbf{A}^{\dagger}\mathbf{b}+\mathbf{A'}^{\dagger}\mathbf{b'}) \\ & +(\mathbf{b}^{\dagger}\mathbf{A}+\mathbf{b'}^{\dagger}\mathbf{A'})\mathbf{w}+||\mathbf{b}||^2+||\mathbf{b'}||^2. \end{array} \tag{3.26}$$

From (3.26), we can obtain the solution of the optimal window $\mathbf{w}$ that minimizes the total interference by differentiating J with respect to $\mathbf{w}$. We have

$$\mathbf{w} = -[Re(\mathbf{A}^{\dagger}\mathbf{A} + \mathbf{A}'^{\dagger}\mathbf{A}')]^{-T}[Re(\mathbf{b}^{\dagger}\mathbf{A} + \mathbf{b}'^{\dagger}\mathbf{A}')]^{T}. \tag{3.27}$$

where notation $Re(X)$ denote the real part of X. The matrices $\mathbf{A}$ and $\mathbf{A}'$, and vectors $\mathbf{b}$ and $\mathbf{b}'$ are shown in detail in [16].

3.2.2 Joint window and TEQ design

We will briefly review the method given in [13]. We consider the case of per tone equalizer and window design. The transmitted QAM frequency domain symbol vector of length M at time k is X^k; its i-th entry is X_i^k. The system model is the same as shown in Fig. 2.1. It is known the i-th input of FEQ can be expressed as

$$Y_{ut,i}^k = \mathcal{F}_M(i,:)\mathbf{U}\mathbf{Y}^{ext,k}\mathbf{t}, \tag{3.28}$$

where $\mathcal{F}_M$ is the DFT matrix, and $\mathcal{F}_M(i,:)$ is the i-th row of $\mathcal{F}_M$; $\mathbf{t}$ is the $T \times 1$ column vector of TEQ coefficients. $\mathbf{Y}^{ext,k}$ is a Toeplitz matrix of received time domain samples y_l^k:

$$\mathbf{Y}^{ext,k} = \begin{pmatrix} y_{-\mu}^k & \cdots & y_{-\mu-T+1}^k \\ \vdots & \ddots & \vdots \\ y_{M-1}^k & \cdots & y_{M-T}^k \end{pmatrix}, \tag{3.29}$$

where μ is the window length. The overall received signal on tone i is determined by the i-th FEQ output, which can be obtained by $D_i Y_{uw,i}^k$. The TEQ design is to minimize the square error between the FEQ output and the transmitted frequency domain symbol. Thus, the objective function is written as:

$$\min E\left[\left|D_i Y_{ut,i}^k - X_i^k\right|^2\right]. \tag{3.30}$$

We can further decompose $Y^{ext,k}$ to connect the relation with window and TEQ coefficients. The matrix $\mathbf{U}$ in (3.28) can be separated into two part $\mathbf{U}_1$ and $\mathbf{U}_2$.

$$\begin{aligned}\mathbf{U} &= \begin{pmatrix} \mathbf{O}_{(M-\mu)\times\mu} & \mathbf{I}_{M-\mu} & \mathbf{O}_{(M-\mu)\times\mu} \\ diag(\mathbf{u}) & \mathbf{O}_{\mu\times(M-\mu)} & \mathbf{I}_\mu - diag(\mathbf{u}) \end{pmatrix} \\ &= \begin{pmatrix} \mathbf{O} & \mathbf{I}_{M-\mu} & \mathbf{O} \\ \mathbf{O} & \mathbf{O} & \mathbf{I}_\mu \end{pmatrix} + \begin{pmatrix} \mathbf{O} & \mathbf{O} & \mathbf{O} \\ diag(\mathbf{u}) & \mathbf{O} & -diag(\mathbf{u}) \end{pmatrix} \\ &= \mathbf{U}_1 + \mathbf{U}_2. \end{aligned} \tag{3.31}$$

For example, the input of DFT after windowing and TEQ filtering is now the result of the product $\mathbf{U}\mathbf{Y}^{ext,k}\mathbf{t}$. Windowing without TEQ filtering is represented by $\mathbf{U}\mathbf{Y}^{ext,k}\left[1\ 0\ \ldots\ 0\right]^T$, while TEQ filtering without windowing is denoted by $\mathbf{U}_1\mathbf{Y}^{ext,k}\mathbf{t}$.

Starting from the definition for $Y^k_{ut,i}$ in (3.28) and applying (3.31), we can write

$$\begin{aligned} Y^k_{ut,i} &= \mathcal{F}_M(i,:)(\mathbf{U}_1+\mathbf{U}_2)\mathbf{Y}^{ext,k}\mathbf{t} \\ &= \mathbf{Y}^{sl,k}_i\mathbf{t} + \Delta\mathbf{y}^{ext,k^T}\mathbf{U}_i\mathbf{t}, \end{aligned} \tag{3.32}$$

where $\mathbf{Y}^{sl,k}_i = \mathcal{F}_M(i,:)\mathbf{Y}^{ext,k}$, and $\Delta\mathbf{y}^{ext,k^T} = \left[\Delta y^k_{-T+1}\ \ldots\ \Delta y^k_{\mu-1}\right]$, $\Delta y^k_{\mu-l} = y^k_{-l} - y^k_{M-l}$.

Notice that the first term of (3.32) can be written as a linear combination of Y^k_i and $T-1$ difference terms $\Delta y^k_{\mu-T+1},\ \ldots,\ \Delta y^k_{\mu-1}$. When the joint window and TEQ operation in $\mathbf{U}_i\mathbf{t}$ is replaced by one tone-dependent vector of unknown, it is easy to see that the second term in (3.32) also comprises a linear combination of the difference terms $\Delta y^k_{-T+1},\ \ldots,\ \Delta y^k_{\mu-1}$. As a consequence, (3.32)can be written in general as a linear combination of the DFT output Y^k_i and $\mu+T-1$ real-valued difference term $\Delta y^{ext,k}$, i.e.,

$$Y^k_{ur,i} = \bar{\mathbf{v}}^T_i\left[\Delta\mathbf{y}^{ext,k^T}\ Y^k_i\right]^T, \tag{3.33}$$

where $\bar{\mathbf{v}}_i$ are now the $\mu+T-1$ unknown coefficients. After applying (3.33) to

(3.30), we obtain

$$\min E\left[\left|D_i\bar{\mathbf{v}}_i^T\left[\Delta\mathbf{y}^{ext,k^T}\ Y_i^k\right]^T - X_i^k\right|^2\right]. \tag{3.34}$$

$D_i\bar{\mathbf{v}}_i$ corresponds to the constraint MMSE solution of $\mu+T$-taps PTEQ design problem. We can also apply orthogonality principle to solve MMSE problem, i.e.,

$$E\left[D_i\bar{\mathbf{v}}_i^T\mathbf{b}_i(D_i\bar{\mathbf{v}}_i^T\mathbf{b}_i - X_i^k)^\dagger\right] = 0, \tag{3.35}$$

where $\mathbf{b}_i = \left[\Delta\mathbf{y}^{ext,k^T}\ Y_i^k\right]^T$. Thus, we can obtain $D_i\bar{\mathbf{v}}_i = \mathbf{R}_{\mathbf{b}_i}^{-1}\mathbf{R}_{\mathbf{b}_iX_i}$, where $\mathbf{R}_{\mathbf{b}_i} = E\left[\mathbf{b}_i\mathbf{b}_i^\dagger\right]$, and $\mathbf{R}_{\mathbf{b}_iX_i} = E\left[\mathbf{b}_iX_i^\dagger\right]$.

Chapter 4

Proposed TEQ design method

In this chapter, we will illustrate the design procedure of proposed method. The main idea of proposed method is to consider the capabilities both of TEQ and RFI suppression. In addition to alleviate the influence of the RFI interference, our goal is to achieve high transmission rate simultaneously.

4.1 Incorporation of RFI Suppression

Assume the statistics of interference sources are available. The radio interference is known as the narrow band signal, and for the duration of one DMT symbol, it can be considered as a sum of sinusoids. The interference is modeled as in (3.18), $u(n) = \sum_{l=0}^{J-1} \alpha_l cos(\omega_l n + \theta_l)$, where ω_l is the frequency of the l-th interference source, and α_l and θ_l are the corresponding amplitude and phase. To analyze the effect of interference, we apply an interference-only signal $u(n)$ to the receiver in Fig. 2.7. The output of the kth tone is $e_k(n) = [e_{rfi,k}(n)]_{\downarrow N}$, where

$$e_{rfi,k}(n) = \frac{1}{P_k} \sum_{l=0}^{J-1} \frac{\alpha_l}{2} [r_{1,l}(n) + r_{2,l}(n)],$$

where

$$r_{1,l}(n) = H_k(e^{j\omega_l}) T_k(e^{j\omega_l}) e^{j(\omega_l n + \theta_l)},$$

$$r_{2,l}(n) = H_k(e^{-j\omega_l}) T_k(e^{-j\omega_l}) e^{-j(\omega_l n + \theta_l)}.$$

Note that the decimators do not change the amplitudes. To suppress interference, we can minimize

$$\phi_{rfi,k} = \frac{1}{|P_k|^2} \sum_{l=0}^{J-1} \frac{\alpha_l^2}{4} [|\rho_{k,l}|^2 + |\eta_{k,l}|^2], \tag{4.1}$$

where

$$\rho_{k,l} = H_k(e^{j\omega_l}) T_k(e^{j\omega_l}), \tag{4.2}$$

$$\eta_{k,l} = H_k(e^{-j\omega_l}) T_k(e^{-j\omega_l}). \tag{4.3}$$

Notice that the equations in (4.2) and (4.3) can be expressed as $\rho_{k,l} = \tau_{k,l}\mathbf{t}_k$, $\eta_{k,l} = \zeta_{k,l}\mathbf{t}_k$, where

$$\begin{aligned} \tau_{k,l} &= H_k(e^{j\omega_l})[1 \; e^{-j\omega_l} \; \ldots \; e^{-j\omega_l(T-1)}] \\ &= \tfrac{e^{j\omega_l\nu}(1-e^{j\omega_l M})}{1-e^{j(\omega_l - \frac{2\pi}{M}k)}}[1 \; e^{-j\omega_l} \; \ldots \; e^{-j\omega_l(T-1)}], \end{aligned} \tag{4.4}$$

$$\begin{aligned} \zeta_{k,l} &= H_k(-e^{j\omega_l})[1 \; e^{j\omega_l} \; \ldots \; e^{j\omega_l(T-1)}] \\ &= \tfrac{e^{-j\omega_l\nu}(1-e^{-j\omega_l M})}{1-e^{-j(\omega_l + \frac{2\pi}{M}k)}}[1 \; e^{j\omega_l} \; \ldots \; e^{j\omega_l(T-1)}]. \end{aligned} \tag{4.5}$$

Using the above derivations, $\phi_{rfi,k}$ in (4.1) can be rewritten as:

$$\frac{\mathbf{t}_k^\dagger \mathbf{Q}_{rfi,k} \mathbf{t}_k}{\mathbf{t}_k^\dagger \mathbf{B}_k \mathbf{t}_k}, \tag{4.6}$$

where $\mathbf{B}_k$ is as in (3.9) and $\mathbf{Q}_{rfi,k}$ is

$$\mathbf{Q}_{rfi,k} = \frac{1}{4} \sum_{l=0}^{J-1} \alpha_l^2 [\tau_{k,l}^\dagger \tau_{k,l} + \zeta_{k,l}^\dagger \zeta_{k,l}]. \tag{4.7}$$

Remark. RFI interference also can be modeled as a random signal just like noise. The error variance caused by RFI interference can be written as $\sigma_{rfi,k}^2 = \frac{\mathbf{t}_k^\dagger \mathbf{Q}_{rfi,k} \mathbf{t}_k}{\mathbf{t}_k^\dagger \mathbf{B}_k \mathbf{t}_k}$, where $\mathbf{Q}_{rfi,k}$ is the same as $\mathbf{Q}_{noise,k}$, but $\mathbf{R}_v$ is replaced with $\mathbf{R}_u$.

4.2 The optimal TEQ

Base on the TEQ design method in section 3.1.2. An objective function that minimizes ISI, noise variance and RFI interference is

$$\phi_k = \sigma^2_{isi,k} + \sigma^2_{noise,k} + \phi_{rfi,k} = \frac{\mathbf{t}_k^\dagger \mathbf{Q}_k \mathbf{t}_k}{\mathbf{t}_k^\dagger \mathbf{B}_k \mathbf{t}_k}, \tag{4.8}$$

where $\mathbf{Q}_k = \mathbf{Q}_{isi,k} + \mathbf{Q}_{noise,k} + \mathbf{Q}_{rfi,k}$. The optimal TEQ $\mathbf{t}_k$ minimizes the ratio in (4.8) or maximizes its inverse

$$\arg\max_{t_k} \frac{\mathbf{t}_k^\dagger \mathbf{B}_k \mathbf{t}_k}{\mathbf{t}_k^\dagger \mathbf{Q}_k \mathbf{t}_k}, k = 1,\ 2, \ldots,\ M-1. \tag{4.9}$$

We can obtain the optimal TEQs $\mathbf{t}_k$ by finding the eigenvector corresponding to the maximum eigenvalue of $\mathbf{Q}_k^{-1}\mathbf{B}_k$. Notice that the ratio in (4.9) is proportional to signal to interference ratio (SINR) of the kth subchannel. Therefore the optimal TEQ $\mathbf{t}_k$ will maximize the subchannel SINR_k.

Moreover, it is not difficult to verify that $\mathbf{Q}_{isi,M-k} = \mathbf{Q}^*_{isi,k}$, $\mathbf{Q}_{noise,M-k} = \mathbf{Q}^*_{noise,k}$, $\mathbf{Q}_{rfi,M-k} = \mathbf{Q}^*_{rfi,k}$ and $\mathbf{B}_{M-k} = \mathbf{B}^*_k$ for $k = 1,\ 2, \ldots,\ \frac{M}{2} - 1$. For $k = 0$ and $k = \frac{M}{2}$, these matrices are real. Thus, the TEQ coefficients have complex conjugate property, i.e, $t_k = t^*_{M-k}$ for $k = 1,\ 2, \ldots,\ \frac{M}{2} - 1$.

Chapter 5

Numerical Simulation

In this chapter, we will evaluate the performance of the proposed TEQ design algorithm. First we introduce the performance measure and simulation environment in section 5.1 and 5.2. We will show the performance of proposed method and compare the simulation results with the pervious method mentioned in chapter 3.

5.1 Performance Measure

- SIR: It is a good measure for evaluating channel shortening effect. The definition of SIR is

$$\frac{\sum_{i=d}^{d+\nu-1} |h(i)|^2}{\sum_{i=0}^{d-1} |h(i)|^2 + \sum_{i=d+\nu}^{T+L-1} |h(i)|^2}, \tag{5.1}$$

  where $h(i)$ is the coefficients of the equivalent channel response.

- Transmission rate: The number of bits allocated for the ith tone is

$$b_i = \left\lfloor \log_2(1 + \frac{SINR_i}{\Gamma}) \right\rfloor. \tag{5.2}$$

  where SINR_i is the signal to interference and noise ratio of ith tone. Γ is the gap between the channel capacity and the achieved bit rate for a given

error rate. The value of Γ depends on desired error rate. For example, all the simulations in this thesis, error rate $P_e = 10^{-5}$ and $\Gamma = 8.1317$. The transmission rate is given by

$$\frac{1}{NT_s}\sum_{i=0}^{M/2} b_i = \frac{1}{NT_s}\sum_{i=0}^{M/2} \left\lfloor \log_2(1 + \frac{SINR_i}{\Gamma}) \right\rfloor . \tag{5.3}$$

In VDSL specification, the maximum number of bits on each tone is 15, and the minimum number of bits on each tone is 2.

5.2 Simulation Environment

They are simulated using VDSL loops 1-7 [2]. The DFT size $M = 1024$, cyclic prefix length $\nu = 80$ and the sampling rate $F_s = 4.416$ MHz. The PSD of transmission is -60 dBm/Hz. The channel noise is additive white Gaussian noise of -140 dBm/Hz and also NEXT and FEXT crosstalk. The RFI interference is of -55 dBm differential mode (the distance between client and interference source is 6000 ft) [2]. In Table. 5.1, it shows seven types of VDSL test loops in our simulation, and their magnitude response are shown in Fig. 5.1.

Table 5.1: VDSL test loop length.

Loop	Length (ft.)
VDSL-1L	4500
VDSL-2L	4750
VDSL-3L	4750
VDSL-4L	4800
VDSL-5	950
VDSL-6	3250
VDSL-7	4900

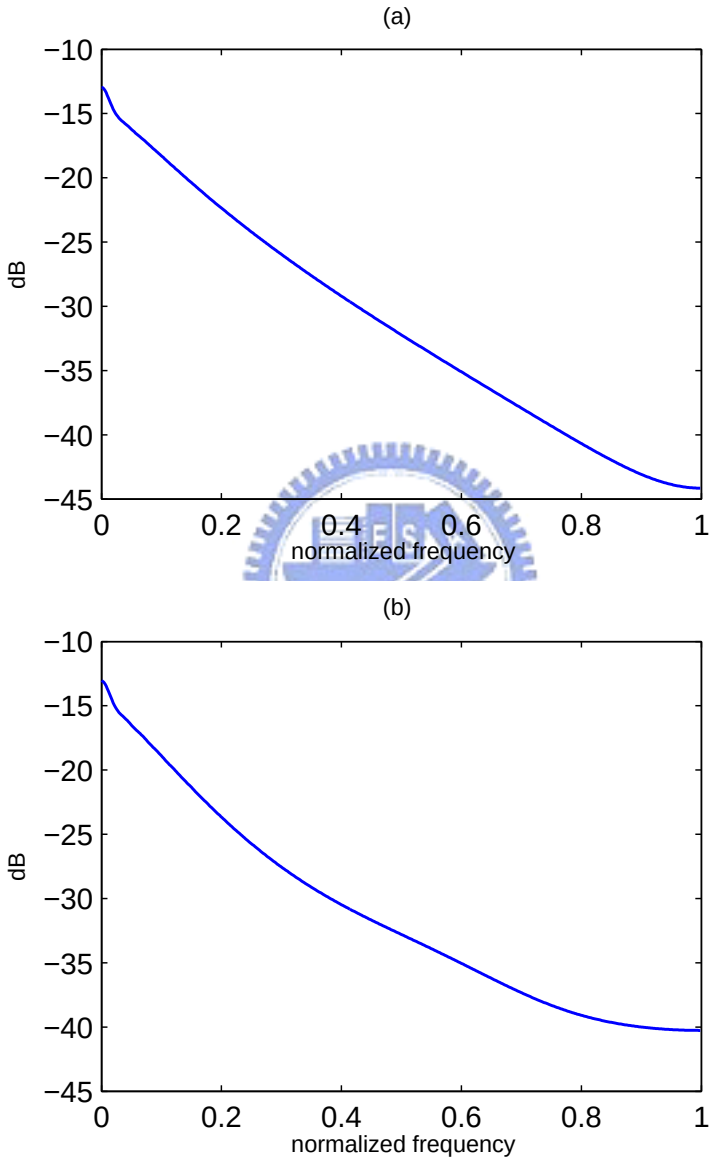
(a)
−10
−15
−20
−25
−30
−35
−40
−45
dB
0
0.2
0.4
0.6
0.8
1
normalized frequency
(b)
−10
−15
−20
−25
−30
−35
−40
−45
dB
0
0.2
0.4
0.6
0.8
1
normalized frequency

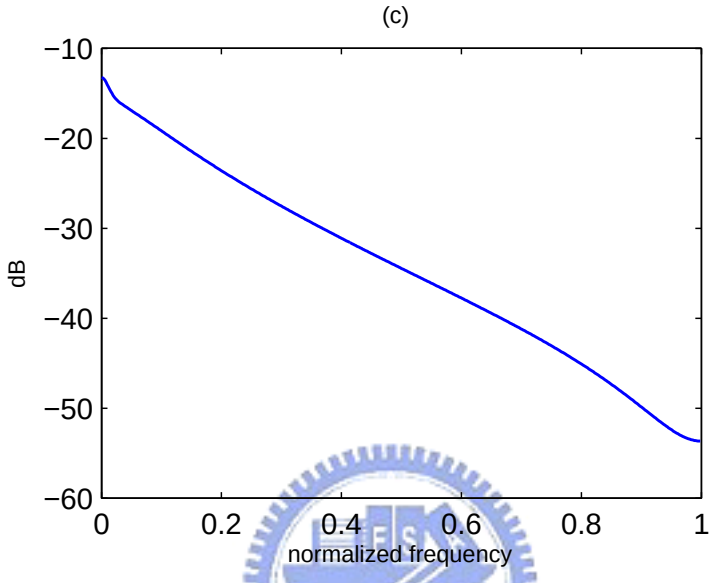
(c)
−10
−20
−30
−40
−50
−60
dB
0
0.2
0.4
0.6
0.8
1
normalized frequency

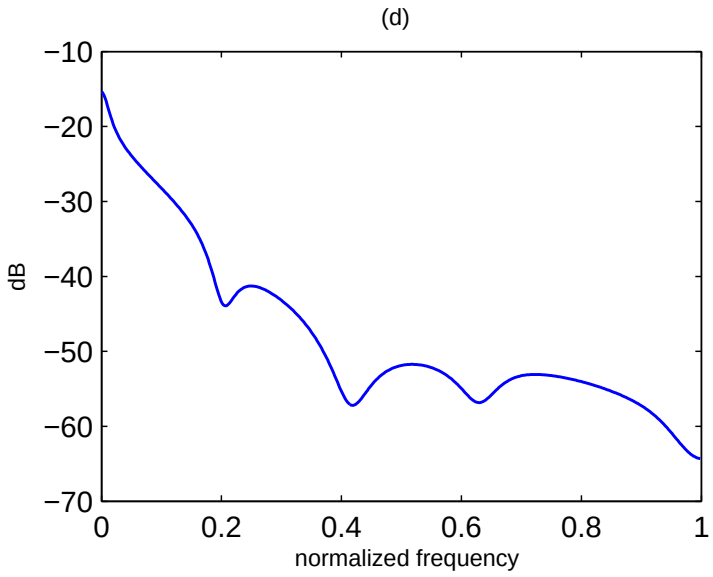
(d)
−10
−20
−30
−40
−50
−60
−70
dB
0
0.2
0.4
0.6
0.8
1
normalized frequency

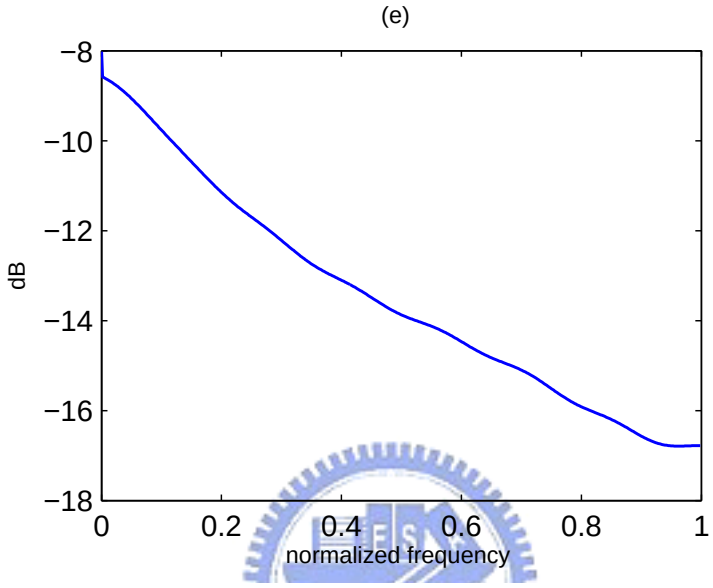
(e)
−8
−10
−12
−14
−16
−18
dB
0
0.2
0.4
0.6
0.8
1
normalized frequency

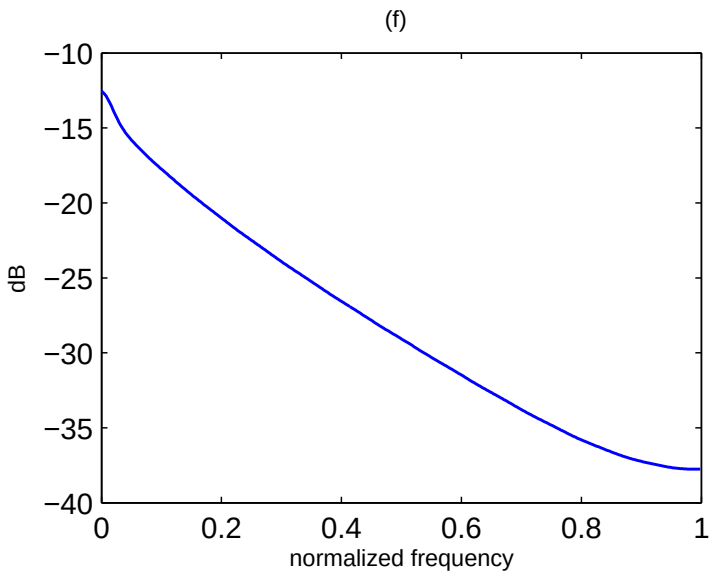
(f)
−10
−15
−20
−25
−30
−35
−40
dB
0
0.2
0.4
0.6
0.8
1
normalized frequency

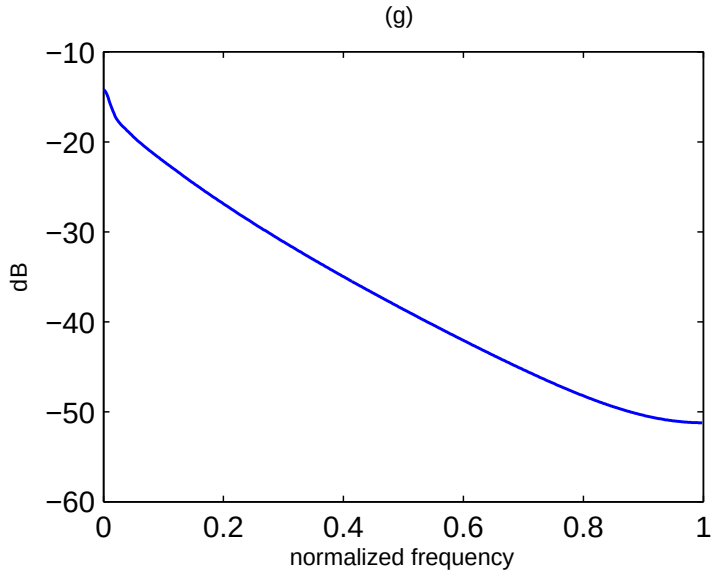

Figure 5.1: The magnitude response of test channel(a)VDSL-1L. (b)VDSL-2L. (c)VDSL-3L. (d)VDSL-4L. (e)VDSL-5. (f)VDSL-6. (g)VDSL-7.

5.3 Simulation Results

In our simulation, we assume the RF interference are of frequencies 1.05MHz, 1.9MHz and 2.0MHz. For the case of $M = 1024$, the corresponding tone indices are the 244, 435 and 461. Fig. 5.2 shows the magnitude response of TEQ of some arbitrary tones, e.g. $\mathbf{t}_{50}$, $\mathbf{t}_{136}$, ..., $\mathbf{t}_{508}$. In these figures, we can see a remarkable phenomenon that the magnitude responses of these TEQs have nulls in RFI frequencies, so that we can achieve the purpose of RFI suppression.

Let us take VDSL loop4 as an example, and choose one of the TEQs arbitrarily to illustrate. The tone index to be chosen is 165. Fig. 5.3(a) shows the real part of shortened channel coefficients of the 165-th tone along with the original channel, and Fig. 5.3(b) shows the image part of shortened channel coefficients of the 165-th tone along with the original channel. Fig. 5.3(c) shows the absolute value of shortened channel coefficients of the 165-th tone along with the original channel,

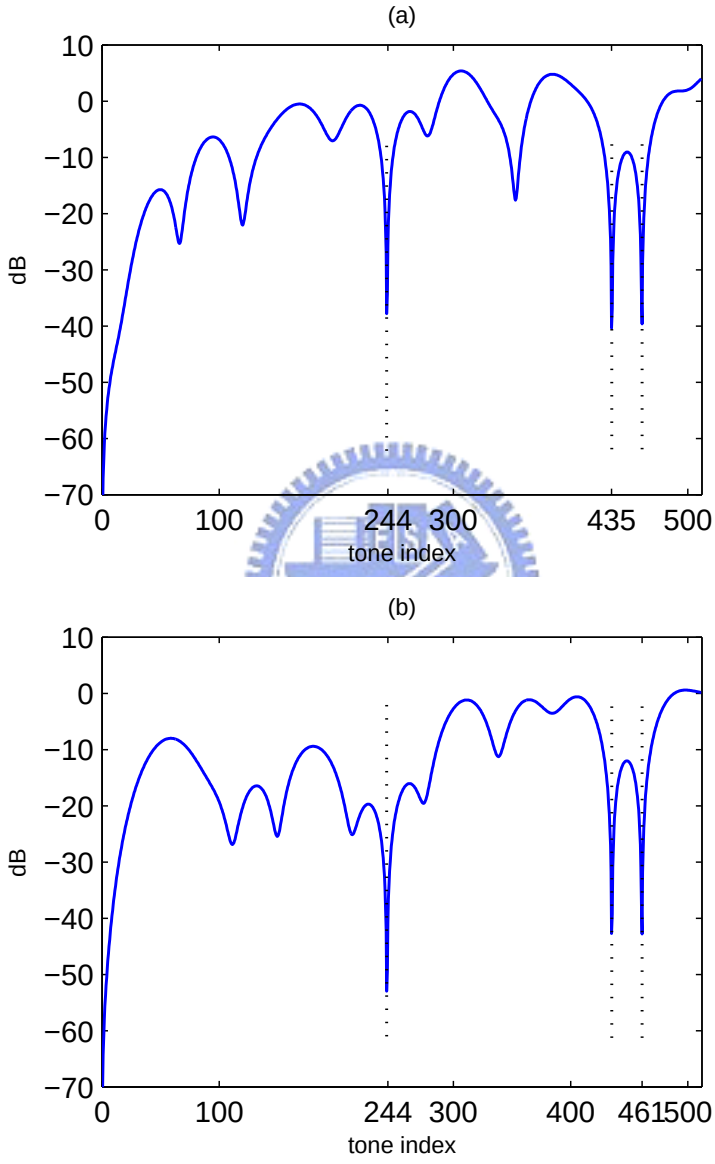
(a)
10
0
−10
−20
−30
−40
−50
−60
−70
dB
0
100
244
300
435
500
tone index
(b)
10
0
−10
−20
−30
−40
−50
−60
−70
dB
0
100
244
300
400
461
500
tone index

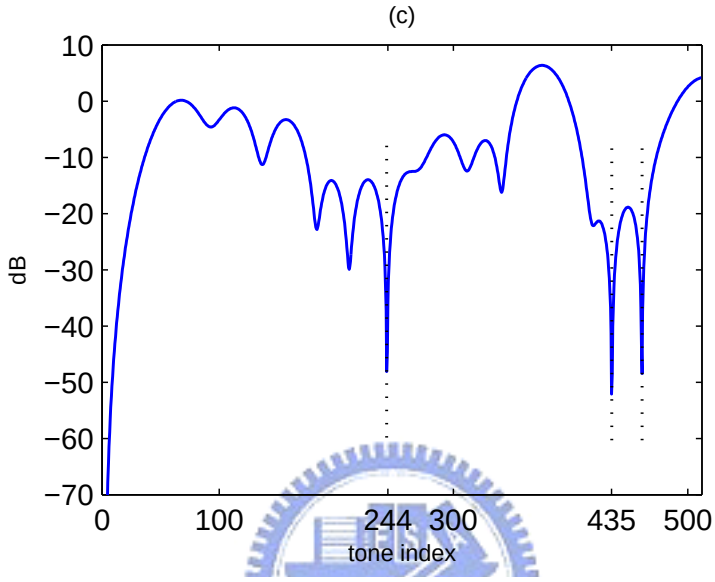
(c)
10
0
−10
−20
−30
−40
−50
−60
−70
dB
0
100
244
300
435
500
tone index

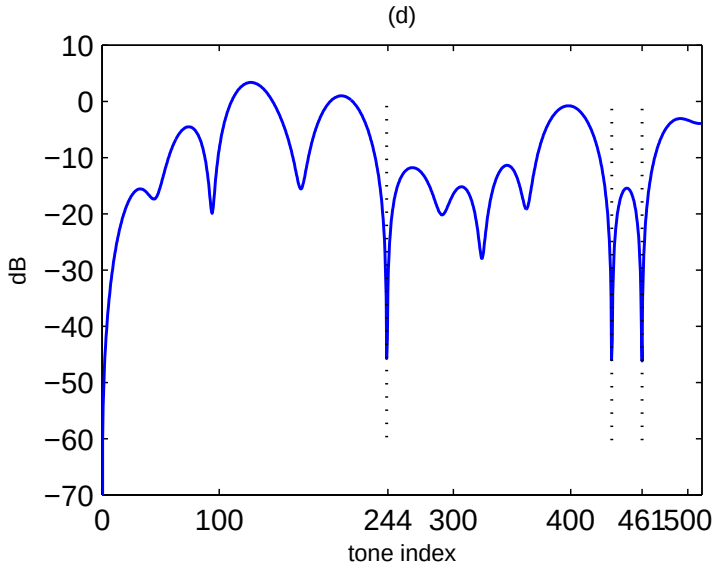
(d)
10
0
−10
−20
−30
−40
−50
−60
−70
dB
0
100
244
300
400
461
500
tone index

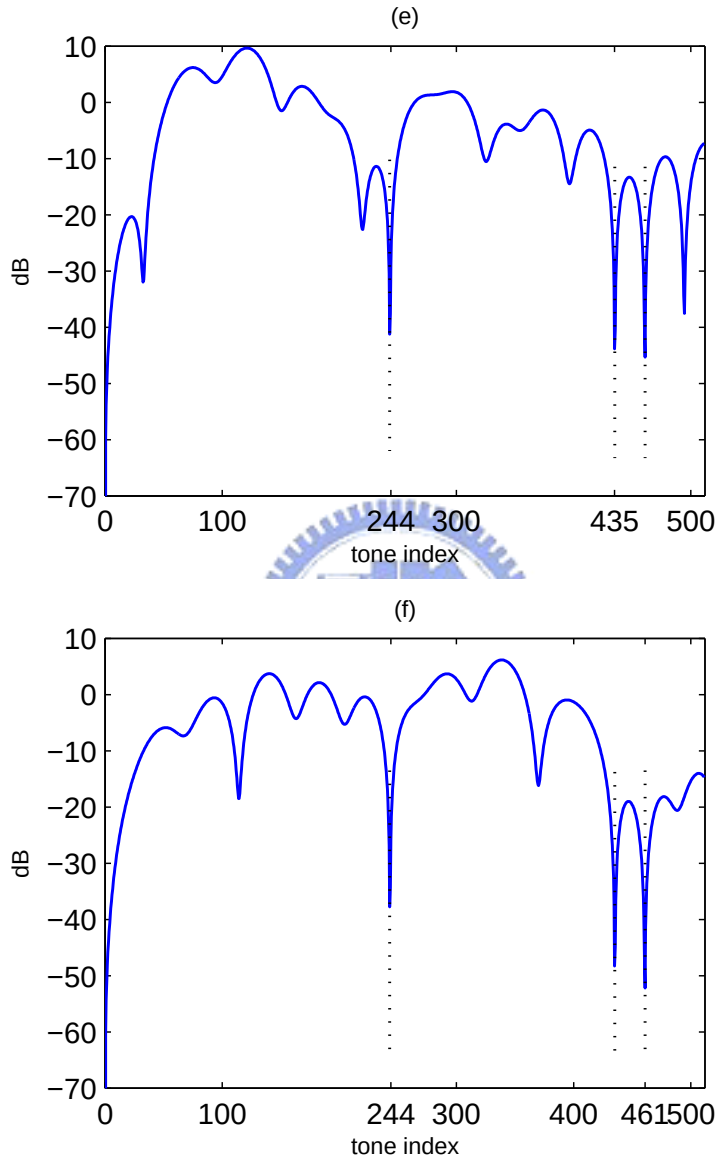

Figure 5.2: The magnitude response of (a)$\mathbf{t}_{50}$. (b)$\mathbf{t}_{136}$. (c)$\mathbf{t}_{227}$. (d)$\mathbf{t}_{309}$. (e)$\mathbf{t}_{467}$. (f)$\mathbf{t}_{508}$. The test channel is VDSL-1L.

and Fig. 5.3(d) shows the magnitude response of shortened channel along with the original channel. Table. 5.2 shows the SIRs of using proposed method, MSSNR [3] and original channel.

Table 5.2: SIR performances on VDSL loops.

VDSL loop	proposed	MSSNR	original
VDSL-1L	71.9	88.9	47.5
VDSL-2L	65.2	90.5	49.7
VDSL-3L	73.9	87.8	43.3
VDSL-4L	60.3	65.4	28.6
VDSL-5	76.8	79.8	35.6
VDSL-6	74.1	85.6	53.2
VDSL-7	67.7	72.5	35.6

Table. 5.3 shows the transmission rate of the proposed method. For comparison, we have shown the performance of windowing methods with a single TEQ. We have shown the cases of rectangular, Hanning, and Blackman windows as well as the window design in [16]. The lengths of window and the TEQ are 10 and 20, respectively. The transmission rate is computed using (5.3).

Table 5.3: Comparison of transmission rate (Mbits/sec) on VDSL loops.

VDSL loop	proposed	[16]	Blackman	Hanning	Rectangular	[13]
VDSL-1L	23.8	20.3	19.7	19.7	19.1	11.6
VDSL-2L	24.1	20.0	19.6	19.5	18.8	10.2
VDSL-3L	22.0	18.5	18.0	18.1	17.3	10.2
VDSL-4L	13.5	10.8	10.4	10.4	9.5	3.0
VDSL-5	28.6	26.9	26.8	26.8	26.6	21.1
VDSL-6	25.5	22.4	21.9	21.9	21.3	11.9
VDSL-7	20.4	17.3	16.8	16.9	16.0	8.6

To gain further insight, in Fig. 5.4, we show the subchannel SINRs around the RFI source frequencies for loop 1. We see that the RFI on the subchannels

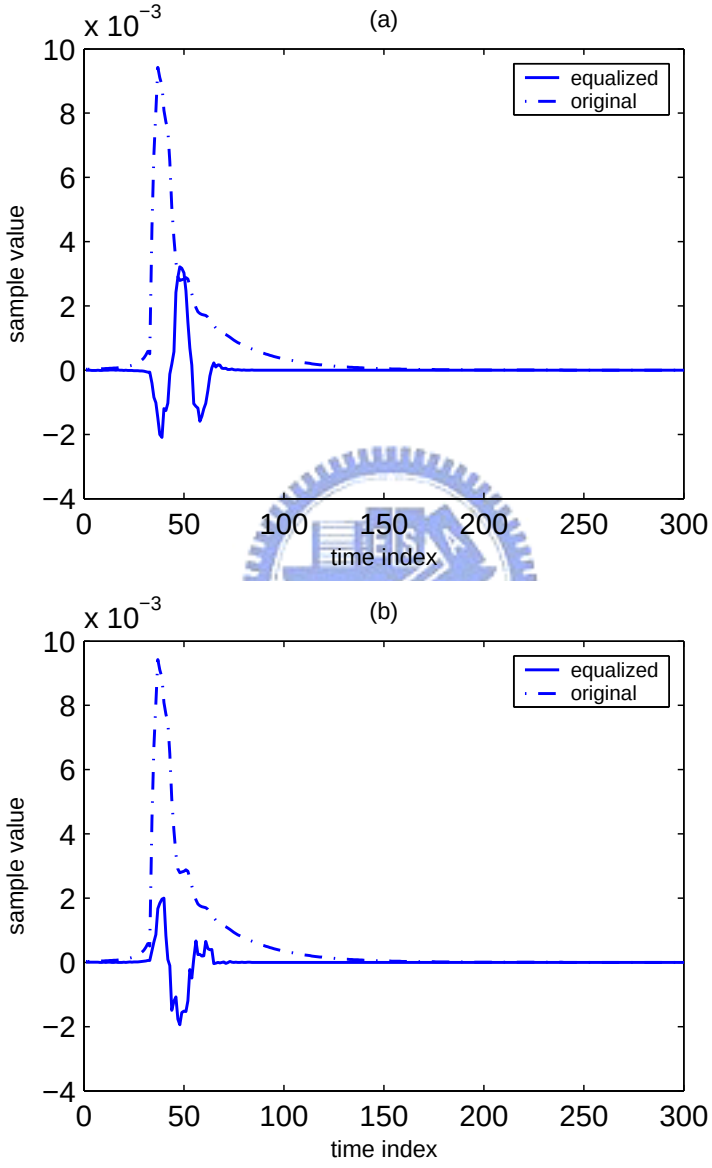
(a)
x 10^−3
10
8
6
4
2
0
−2
−4
sample value
0
50
100
150
200
250
300
time index
equalized
original
(b)
x 10^−3
10
8
6
4
2
0
−2
−4
sample value
0
50
100
150
200
250
300
time index
equalized
original

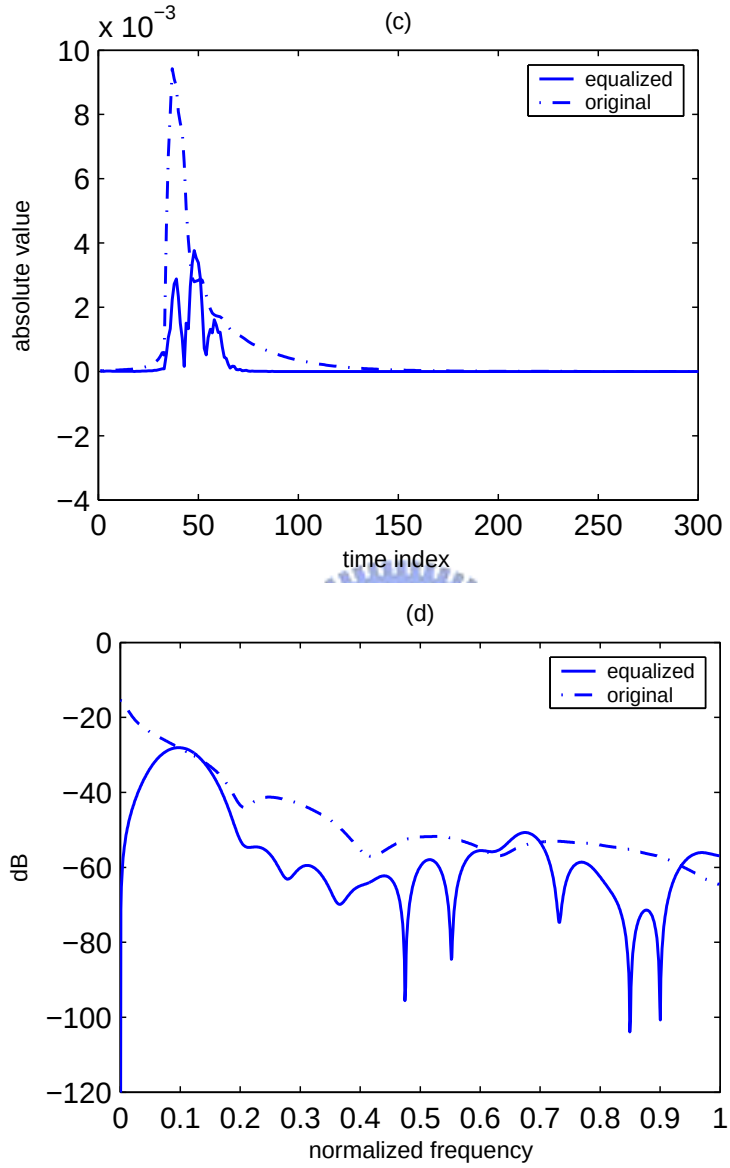

Figure 5.3: The test loop is VDSL-4L. (a) The real part of shortened channel coefficients of the 165th tone. (b) The image part of shortened channel coefficients of the 165th tone. (c) The absolute value of shortened channel coefficients of the 165th tone. (d) The magnitude response of shortened channel along with the original channel.

near the RFI source can be significantly reduced. Thus, we can transmit more bits in those subchannels and a higher transmission rate is achieved.

The performance of the proposed design with different TEQ length is shown in Table. 5.4. The Transmission rate saturates when the length $\geq$20. That is, we can use fewer taps to achieve the same results and lower the complexity of computation simultaneously. Fig. 5.5 shows the subchannel SINRs of the proposed method with different length.

Table 5.4: Transmission rates (Mbits/sec) of the proposed design with different TEQ length on VDSL loop1 (4500ft).

TEQ length	10	15	20	25	30
bit-rate	23.2	23.7	23.8	23.8	23.8

Example. PTEQ v.s. proposed TEQ :

In this example, we simulate the interference of the the DMT system at the frequency domain equalizer (FEQ) output for PTEQ [7] and the proposed TEQ. The simulation environment is the same as described in section. 5.2. We show the powers of signal, ISI, AWGN, crosstalk (FEXT and NEXT) and RFI interference in Fig. 5.6 when PTEQ is implemented and in Fig. 5.7 when the proposed TEQ is implemented. Compare Fig. 5.6 with Fig. 5.7, in the case of PTEQ, the RFI interference is dominating and the signal to interference and noise ratio (SINR) is considerably decreased. In the case of proposed TEQ, the RFI interference is significantly suppressed and the other interference (AWGN, ISI, FEXT and NEXT) is similar to the case of PTEQ. The SINRs of individual tones for PTEQ and proposed TEQ are shown in Fig. 5.8.

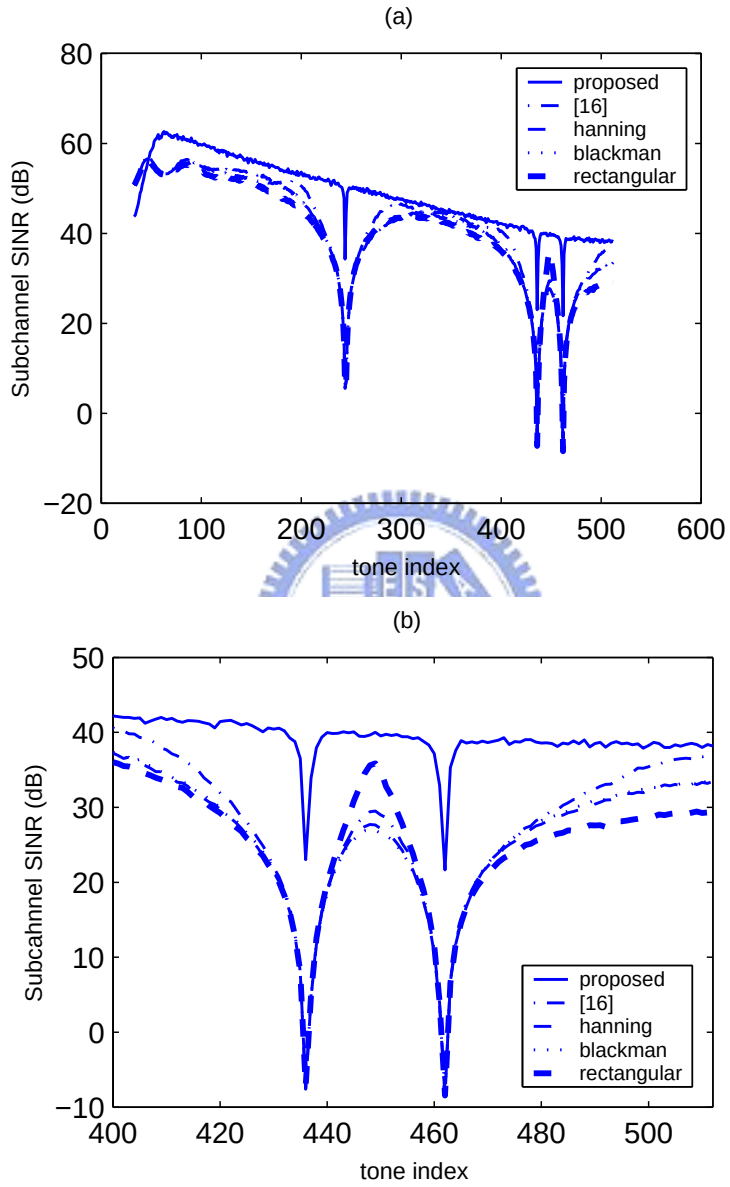

Figure 5.4: (a)The SINRs of individual tones. (b) A zoom-in of (a).

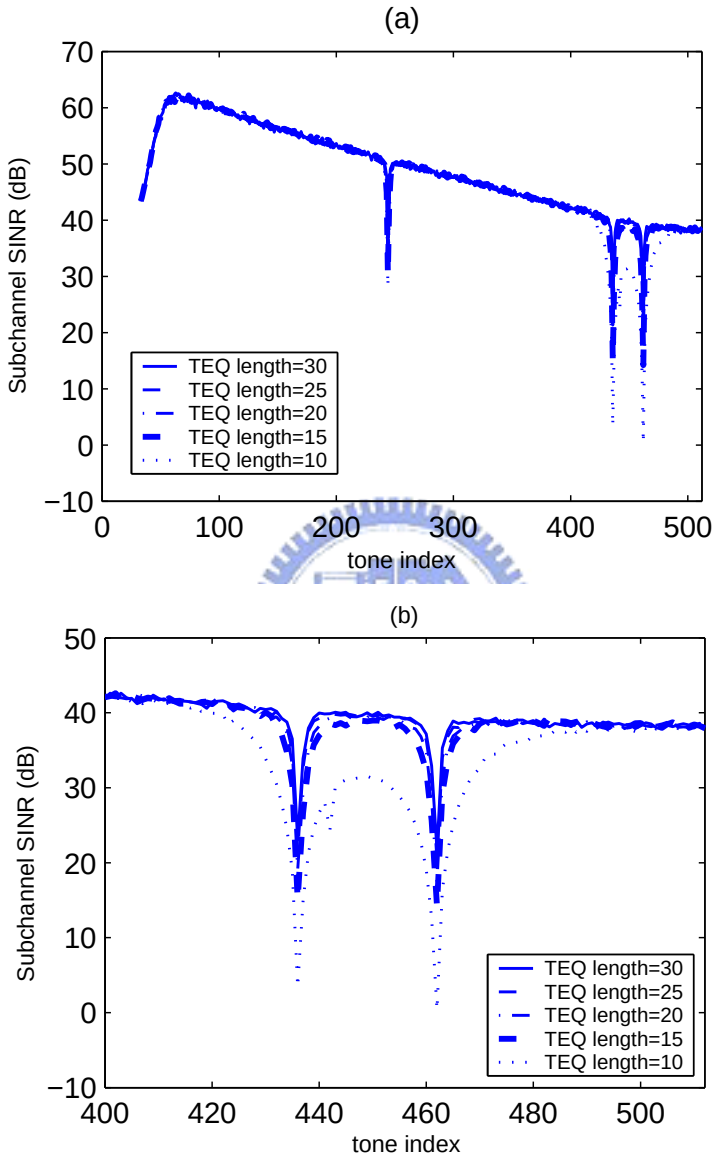

Figure 5.5: (a) Subchannel SINRs of the proposed method with different length. (b) A zoom-in of (a).

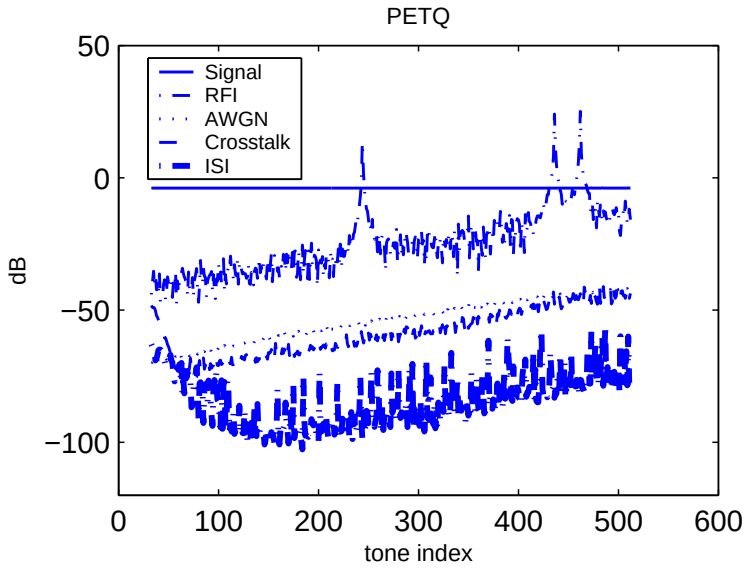

Figure 5.6: The powers of signal, ISI, AWGN, crosstalk and RFI interference at FEQ output when PTEQ is implemented.

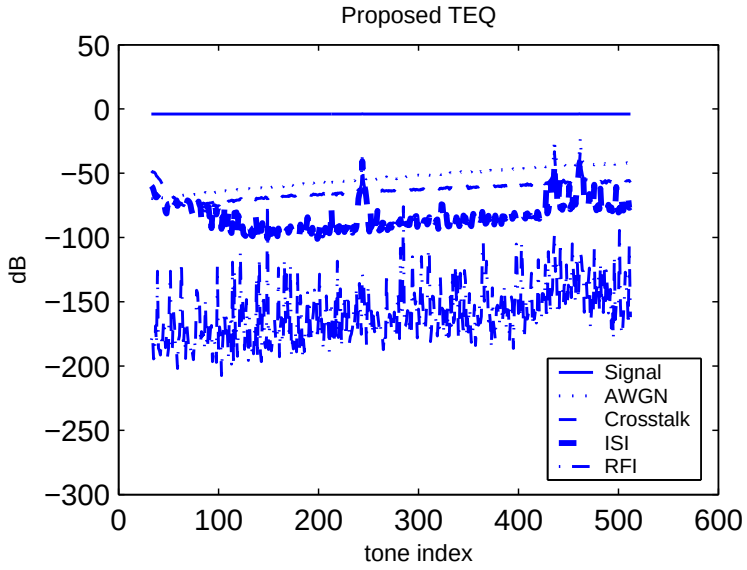

Figure 5.7: The powers of signal, ISI, AWGN, crosstalk and RFI interference at FEQ output when proposed TEQ is implemented.

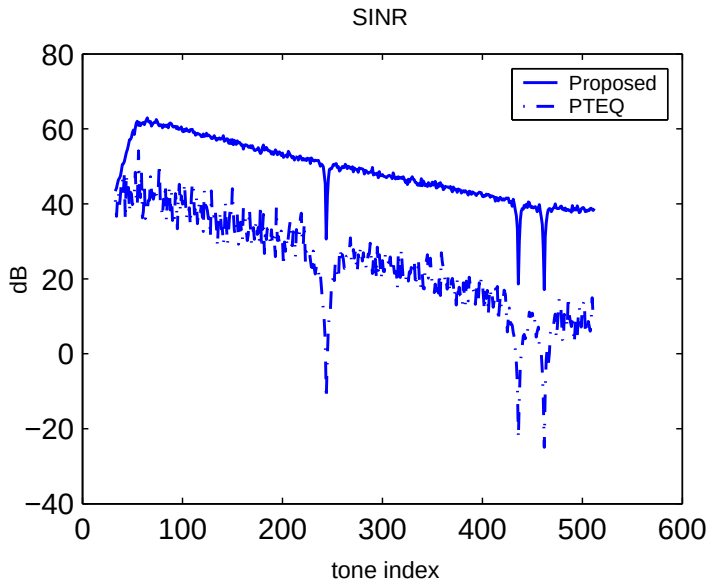

Figure 5.8: The SINRs of individual tones in the case of PTEQ and proposed TEQ.

Example. Joint window and TEQ design v.s. proposed TEQ :

In this example, we simulate the transmission rate of the DMT system using the proposed TEQ and compare with the joint window in [13]. Table. 5.5 shows the transmission rates. The simulation environment is the same as that described in section. 5.2, except for the radio frequency interference (RFI) strength. The transmission power is -60dBm/Hz and the RFI strength is -90dBm. We can see that the proposed TEQ can achieve a higher transmission rate.

Table 5.5: The transmission rate when the transmission power is -60dBm/Hz and the RFI strength is -90dBm.

VDSL loop	loop1	loop2	loop3	loop4	loop5	loop6	loop7
[13]	22.0	23.2	20.8	11.9	27.4	23.8	18.9
proposed	28.5	28.6	28.0	25.1	28.8	28.7	28.0

Table. 5.6 shows the transmission rates when the transmission power is also

-60dBm/Hz, but the RFI strength increases to -55dBm.

Table 5.6: The transmission rate when the transmission power is -60dBm/Hz and the RFI strength is -55dBm.

VDSL loop	loop1	loop2	loop3	loop4	loop5	loop6	loop7
[13]	11.6	10.2	10.2	3.0	21.1	11.9	8.6
proposed	23.8	24.1	22.0	13.5	28.6	25.5	20.4

Examing the simulation results in Table. 5.5 and Table. 5.6, we see that when RFI strength increases, the transmission rate of joint window and TEQ design [13] decreases considerably. However the transmission rate of the proposed TEQ is not affected as seriously. As far as RFI suppression is concerned, the proposed TEQ is more robust than the method of [13].

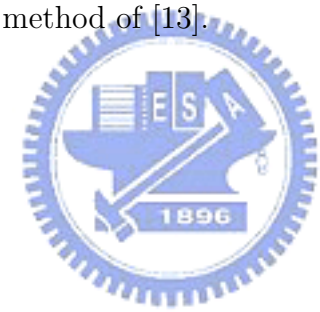

Chapter 6

Conclusion

In this thesis, we use a filterbank formulation for designing TEQ incorporating RFI suppression. The optimal TEQs are obtained by minimizing the ISI, channel noise and RFI interference. The proposed TEQs have nulls at the frequencies of RFI sources. The proposed TEQs can significantly alleviate the effect of RFI for the tones around RFI frequencies. Compare with traditional window design for RFI suppression, the proposed method can achieve larger SINRs and obtain higher transmission rate. We also explore the performance of proposed method with different TEQ length. We can see the transmission rate saturates when the length is smaller than our desired length. Notice that the coefficients of proposed TEQs have symmetric property just like the transmitted symbols, so that the computational complexity can be reduced more. The simulation results demonstrate that larger SINR can be obtained and higher transmission rates can be achieved.

Bibliography

[1] "Asymmetric Digital Subscriber Lines (ADSL)-Metallic Interface", ANSI T1.413, 1998.

[2] "Very-high Speed Digital Subscriber Lines (VDSL)-Metallic Interface", ANSI T1.424, 2002.

[3] Peter J. W. Melsa, Richard C. Younce, Charles E. Rohrs, "Impulse response shortening for discrete multitone transceiver", *IEEE Trans. on Communication,* vol. 44, no.12, pp. 1662-1672, Dec. 1996.

[4] G. Arslan, B. L. Ecans, S. Kiaei, " Equalization for discrete multitone transceivers to maximize bit rate," *IEEE Transactions on Signal Processing,* vol.49, no. 12, pp. 3123-3135, Dec. 2001.

[5] K. Van Acker, G. Leus, M. Moonen, O. van de Wiel, and T. Pollet, " Per tone equalization for DMT-based system," *IEEE Trans. Communications,* vol. 49, no. 1, pp. 109V119, Jan. 2001.

[6] R. K. Martin, J. Balakrishnan, W. A. Sethares, and C. R. Jr. Johnson, "Blind, adaptive cahnnel shortening for multicarrier systems", Signals, Systems and Computers, 2002. Conference Record of Thirty-sixth Asilomar Conference, vol. 1, pp. 372-376, NOV. 2002.

[7] Chun-Yang Chen, and See-May Phoong, "Bit rate optimized time-domain equalizers for DMT systems", Circuits and Systems, 2003. ISCAS '03, vol. 4, pp. IV-37 - IV-40, May 2003.

[8] R. K. Martin, K. Vanbleu, M. Ding, G. Ysebaert, M. Milosevic, B. L. Evans, M. Moonen, and C. R. Johnson Jr., " Unification and Evaluation of Equalization Structures and Design Algorithms for Discrete Multitone Modulation Systems," *IEEE Trans. Signal Processing,* to appear.

[9] L. De Clercq, M. Peeters, S. Schelstraete, T. Pollet, "Mitigation of Radio Interference in xDSL Transmission." IEEE Communications Magazine, vol. 38, no. 3, March 2000.

[10] A. J. Redfern, "Receiver window design for multicarrier communication systems", *IEEE Trans. on Communications,* vol. 20, no. 5, pp. 1029-1036, June 2002.

[11] S. Kapoor and S. Nedic, "Interference suppression in DMT receiver using windowing", in ICC, 2000, pp. 778-782.

[12] G. Cuypers, K. Vanbleu, G. Ysebaert, M. Moonen, "Combining raised cosine windowing and per tone equalization for RFI mitigation in DMT receivers", in ICC, vol.4, pp. 2852-2856, May 2003.

[13] G. Ysebaert, K. Vanbleu, G. Cuypers, and M. Moonen, " Joint Window and Time Domain Equalizer Design for Bit Rate Maximization in DMT-Receivers," *IEEE Journal on Selected Areas in Communication,* vol. 20, no. 5, pp. 1029-1036, June 2002.

[14] J. A. C. Bingham, "RFI Suppression in Multicarrier Transmission System," Global Telecommunications Conference, 1996.

[15] Byung-Jang Jeong and Kyung-Hyun Yoo, "Digital RFI canceller for DMT based VDSL." Electronics Letters, vol. 34, no.17, pp.1640-1641, Aug 1998.

[16] Yuan-Pei Lin, Chien-Chang Li, "Optimal Receiver Window Design For Radio Frequency Interference Suppression", in European Signal Processing Conference, 2006.

[17] P.P. Vaidyanathan, *Multirate Systems and Filter Banks,* Englewood Cliffs, Prentice Hall, 1993.

[18] Alan V.Oppenheim, Ronald W. Schafer, John R. Buck, *Discrete-Time Signal Processing,* Prentice Hall, 1999.